2006

# Exploration of Iron and Cobalt Core-Shell Nanoparticles via Thermal and Microwave Polyol Synthesis

Hope M. Klukovich
*Wright State University*

# EXPLORATION OF IRON AND COBALT CORE-SHELL NANOPARTICLES VIA THERMAL AND MICROWAVE POLYOL SYNTHESIS

A thesis submitted in partial fulfillment
of the requirements for the degree of
Master of Science

By

HOPE MARIE KLUKOVICH
B.A., University of Nevada Las Vegas, 2002

2006
Wright State University

WRIGHT STATE UNIVERSITY

SCHOOL OF GRADUATE STUDIES

October 26, 2006

I HEREBY RECOMMEND THAT THE THESIS PREPARED UNDER MY SUPERVISION BY Hope Marie Klukovich ENTITLED Exploration of Iron and Cobalt Core-shell Nanoparticles via Thermal and Microwave Polyol Synthesis BE ACCEPTED IN PARTIAL FULFILLMENT OF THE REQUIREMENTS FOR THE DEGREE OF Master of Science .

_____

Eric Fossum, Ph.D.
Thesis Director

_____

Kenneth Turnbull, Ph.D.
Department Chair

Committee on Final Examination

_____

David A. Grossie, Ph.D.

_____

Eric Fossum, Ph.D.

_____

Vladomir Katovic, Ph.D.

_____

Joseph F. Thomas, Jr. Ph.D.
Dean of the School of Graduate Studies

## ABSTRACT

Klukovich, Hope Marie M.S., Department of Chemistry, Wright State University, 2006. Exploration of Iron and Cobalt Core-shell Nanoparticles via Thermal and Microwave Polyol Synthesis.

Thermal and microwave polyol methods were investigated in the synthesis of various iron and cobalt core-shell nanoparticles. The reaction involved 1 mmol of an $Fe^{+2}$ or $Co^{+2}$ salt, bis-acetylacetanato [$(Acac)_2$] iron (II), cobalt $(Acac)_2$ or iron (II) acetate along with 1 mmol of a surfactant capping agent. The salt was reduced with 2 mmol of a 1,2 diol. When 1,2-hexadecanediol solid was used as a reducing agent, it was dissolved along with the metal salt and capping agent in octyl ether. When 1,2-hexanediol liquid was used as the reducing agent, it was also the solvent, and octyl ether was eliminated. For reactions in which octyl ether acted as the solvent, the capped nanoparticles were precipitated using ethanol. For reactions in which the solvent also acted as the reducing agent, the particles precipitated after nucleation and supersaturation of the polyol solvent/reducing agent. The effects of reducing agent, capping agent, and heating mechanism were investigated. The thermal polyol method was investigated to reproduce published results and compared against results from the microwave polyol method. Development of a new microwave polyol method was investigated using solvents with higher dielectric constants than those used in the thermal polyol method. Products were characterized using FT-IR, and Powder X-ray Diffraction (XRD) to determine bond breakage and formation and crystal structure. AFM and TEM were used for some products to determine size and morphology.

## TABLE OF CONTENTS

## LIST OF FIGURES

Figure Page

## LIST OF FIGURES (CONTINUED)

Figure Page

## LIST OF FIGURES (CONTINUED)

Figure Page

## LIST OF SCHEMES

Scheme Page

## LIST OF TABLES

Table Page

## ACKNOWLEDGMENTS

I would like to thank Dr. Eric Fossum, Department of Chemistry, Wright State University, Dayton, Ohio, for his patience and guidance through this masters program. He taught me more than I could have asked for about writing and even more about organic chemistry. I would also like to thank Dr. Vladimir Katovic and Dr. David Grossie for teaching me more than an organic chemist should know about inorganic chemistry. The learning experience of my masters thesis would not have been complete without their direction.

Great thanks also goes to my loving husband Steve. Without him complaining about ROTC, I would have thought I had it worse than I did. Thank you for always believing in me. I would also like to thank my mom and dad for being the better parents than I was a kid. Dad, we miss you.

A special thanks goes to the United States Air Force for giving me the opportunity to pursue my masters degree. Bill Harrison was instrumental in allowing the time and money needed to complete this program. Dr. Chris Bunker and Dr. Elena Guliants provided the best research project and environment I could have hoped for. Last but not least, Barbra Harruff, Ryan Schwarb and Kyle Novak helped keep me sane and focused.

# I. INTRODUCTION

## 1.1 Background/Driving-force for Research

Turbine engines convert the kinetic energy from a moving fluid into mechanical energy by using the motion of the fluid to turn the fan blades of a rotor. The rotor is connected to a device that does useful work in that it powers the aircraft forward.[1] the fluid that jet engines use is a hot, pressurized gas produced by the combustion of jet fuel. When the gas escapes from the engine it drives a turbine that drives a compressor that compresses the air entering the engine.[1] By way of Newton's third law, when the hot compressed gas leaves the turbine engine at a high velocity it propels the jet in the opposite direction of the escaping gas.

Jet fuel is an essential component for the combustion process. Current technology does not allow for the complete separation of all the different hydrocarbons found in aviation fuel; by some estimates there are over a thousand. These hydrocarbons are mainly paraffins and aromatics. Based on the concentrations of the different components, the fuel has different thermodynamic properties. For a fuel that contains mostly aromatics, the density will be higher and the energy content by weight will be increased relative to one that contains mostly paraffins or naphthalene.[1]

Different types of aviation fuel contain numerous ranges of carbon numbers and molecular weights associated with the hydrocarbons. JP-8 is the grade of fuel most commonly used by the Air Force for their aircraft. JP-8 is almost completely kerosene with a $\Delta H_{comb}$ of about -46.3kJ/g. This value can only be obtained experimentally due to

the highly complex mixture of hydrocarbons. The amount of heat released per gram of fuel is very important because jets have strict weight limits to maintain. The more energy they can get per unit of weight the better. One of the most desirable properties a jet fuel can possess is a low carbon number. A low carbon number jet fuel equates to less weight, and therefore the jet can carry a heavier payload. In kerosene based fuels the carbon number ranges from about 8 to 16.[1] Different specifications for jet fuels such as freeze point (for high altitude), smoke point, or naphthalene concentration aid in determining the carbon number of the fuel.[1] The main way of separating the different carbon numbers is based on the boiling point of the liquid as the boiling point is directly related to molecular weight.

In the commercial aviation arena, the jet fuel that is used is called Jet-A. On the military side of aviation the fuel used starts out as Jet-A, but an additive package specifically tailored to military flying missions is added. This additive package changes the fuel from Jet-A to JP-8. The additives are normally petroleum based and their chemistries are highly specialized.[1]They are added in very small amounts; in the ppm range. The additives typically found in JP-8 are an antioxidant, an electrical conductivity/static dissipater, a corrosion inhibitor, and an ice inhibitor.[1] There is a more specialized type of JP-8 used in military aircraft known as JP-8 +100. The +100 designation denotes that the thermal stability additive has been added to increase the thermal stability of the fuel by about $100^0$C.[1] The JP-8 +100 fuel is mostly used for high altitude and high mach missions such as those of the SCRAMJET aircraft. These types of high stress missions require a fuel with a higher thermal stability.

Thermal stability is a measure of the amount of heat stress a fuel can withstand before it begins to do damage to the aircraft. Thermal instability leads to the formation of materials such as peroxides, soluble gums and insoluble particulate matter that can coat the inside surfaces of an engine. Not much is known about these instability reactions. However, it is believed that most of them are multi-step oxidation reactions. The reactants are thought to be sulfur and nitrogen containing compounds as well as organic acids and reactive olefins.[1] Trace contaminant metals may act as catalysts for these reactions.

In addition to powering the engine through combustion, fuel also acts as a heat sink for the heat generated by the aircraft's engine and other moving parts. Because an aircraft does not have a radiator like a car, the fuel is used to remove the potentially damaging heat by acting as a heat exchange medium. The heating of the fuel can initiate reactions that can leave harmful deposits on the inside of the engine.[1] Thus, the issue of thermal stability becomes an important and limiting factor for aircraft.

It is difficult to measure thermal stability because it is an intangible parameter. There are many indirect ways of measuring thermal stability such as smoke point and, more commonly, freeze point. There is a strong correlation with lowering the freeze point of the fuel and increasing the thermal stability. Differential scanning calorimetry (DSC) has been used to investigate thermal stability by studying phase transitions and transition enthalpies.[2]

Dissolved oxygen in fuel decreases thermal stability because it triggers a chain of oxidation reactions, which produce harmful build up on engine parts such as the fuel nozzle. If the fuel nozzle becomes clogged, it becomes difficult to create the correct

mixture of fuel and air for combustion, which can lead to engine stall or failure. Approved anti-oxidants, typically hindered phenols such as 2,6-di-*tert*-butyl-4-methyl phenol, are currently added to most hydrotreated fuels to prevent oxidation chain reactions.[1]

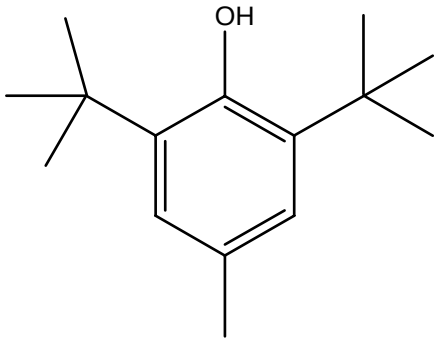


**Figure 1.1** 2,6-ditertiary butyl-4-methyl phenol

Antioxidants work by interrupting the oxidation chain reactions set off by a small amount of dissolved oxygen, thereby preventing the formation of peroxides, soluble gums, or insoluble particulates. These anti-oxidants do not increase the thermal stability of the fuel, and are mainly used for improving storage stability.[1] Recent work has focused on creating an anti-oxidant that can also increase thermal stability. One of the most promising types of research in this area has come from nanotechnology.

## 1.2 Nanotechnology

Nanoscience is a rapidly expanding field of science and engineering. The study of nanoscience leads to new developments in nanotechnology. Nanotechnology is the development and manipulation of materials on the 1-100 nm scale. To get an idea of how small that is, a sheet of a paper is about 100,000 nm thick. Materials of this size are particularly interesting because of their inherent chemical and physical properties.

Because of a high surface-to-volume ratio, nanoparticles are very sensitive to surface environments. The aim of nanotechnology is to better understand these properties and find new ways of utilizing them.

The relatively new field of nanotechnology is attempting to solve the problems associated with dissolved oxygen in jet fuel. Nanomaterials have been the focus of a great deal of study because they possess interesting optical, electrical, magnetic and chemical properties.[3] These interesting properties are attributed to the fact that these materials exhibit much different characteristics than when in bulk.[3] For example, because these particles have a large surface area relative to the number of atoms they contain, there is a notable effect on the cohesive interactions between particles. The increase in cohesive interactions has been shown to decrease the melting temperature as the diameter of the nanoparticle decreases.[4,5] Particles that possess such a small diameter are in an intermediate state between bulk and molecular states.[6] Due to the vast interface between the nanoparticle and the surrounding medium, the medium can have a profound influence on the physical and chemical properties of the nanoparticle making it well suited for chemically selective sensing.[5] Advances in facile synthesis techniques for ordered nanostructures are essential for producing novel nanodevices.

There are many different methods of producing nanoparticles such as sonochemical, micellular, coprecipitation and microemulsion, and laser pyrolysis.[7] Most often, metal nanoparticles are formed in the presence of surfactants, which bond to the surface of the particles, or "cap" the particles. Thiols have been used most extensively for coating metals and metal oxides.[8] Carboxylic acids such as oleic acid and amines such as oleylamine are of much interest as capping agents. These capping agents are useful in the

fabrication of metal nanoparticles because of their lubrication, catalysis, and corrosion resistance properties.[8,9] These surfactants play a very important role in the successful formation of certain metal nanoparticles such as cobalt. It is difficult to prepare Co nanoparticles without surfactant materials because the attractive forces between the particles are large.[10]

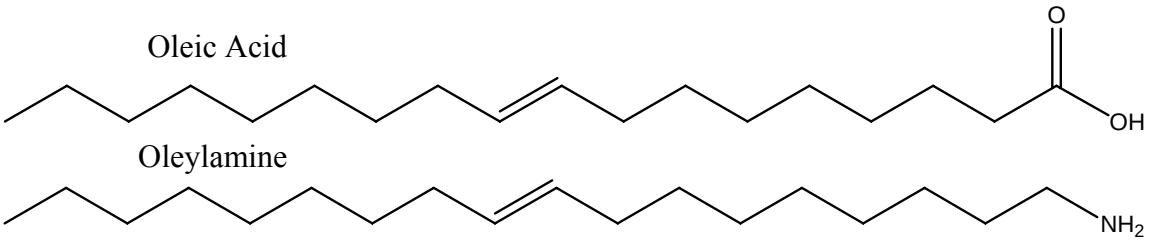


**Figure 1.2** Common capping agents used in metal nanoparticle syntheses

There are many published reports as to how these amphiphilic molecules bond to the surface of metals. These capping agents have been described as adsorbing to the surface of the nanoparticle spontaneously when the particle is directly exposed to the capping agent, and any ordering of the molecules that occurs is spontaneous.[9] The structure of this layer of capping agent can depend on the type of metal it is bonding to as well as the chain length of the capping agent. Depending on the type of metal the capping agent is binding to, this bond formation can be described by three types of bonding. 1) the acid forms a metal carboxylate salt, 2) the acid is chemisorbed via proton transfer to a lattice oxygen atom, and 3) the acid is chemisorbed with no proton transfer, in other words, hydrogen bonded.[9] The mechanism by which the capping agent bonds to the surface can affect particle shape and size. In turn, particle shape and size affect the chemical properties of the nanoparticle, therefore, it is very important to be able to control the size and shape of the particles.[11]

The capping agents bond to the surface of various metals differently. For example, on silver surfaces, the carboxylate is bound to the surface through both oxygen atoms.[8] It has been reported that an ionic bond exists between the carboxylic acid head group and the metallic ions on the surface of iron oxide nanoparticles.[8] The FT-IR region which indicates a chemical bond between the organic acid and the metal surface has been formed is the $\nu$(C=O) stretching mode. This band is observed at 1706 $cm^{-1}$ for nonadecanoic acid, but after it has bonded to a metal substrate, the $\nu$(C=O) stretching is observed in two bands at 1593 and 1440 $cm^{-1}$.[8] These two bands correspond to the symmetric and asymmetric $\nu$(C=O) stretches, respectively. The presence of both of these $\nu_s$(C=O) and $\nu_a$(C=O) stretching modes indicates that a portion of the carboxylate head-groups are bonded to the metal surface at an angle. There are also two bands in the 2850-2960 $cm^{-1}$ region that are associated with the $CH_2$ symmetric and asymmetric stretching.[8] These bands can also be used to verify that the capping agent is still present after reaction. If only the symmetric stretching, $\nu_s$(C=O) is observed in the form of a single band at around 1404 $cm^{-1}$, this indicates the organic acid is bonded to the surface of the metal via a bridged metal-oxygen-carbon-oxygen-metal bond.[8,12]

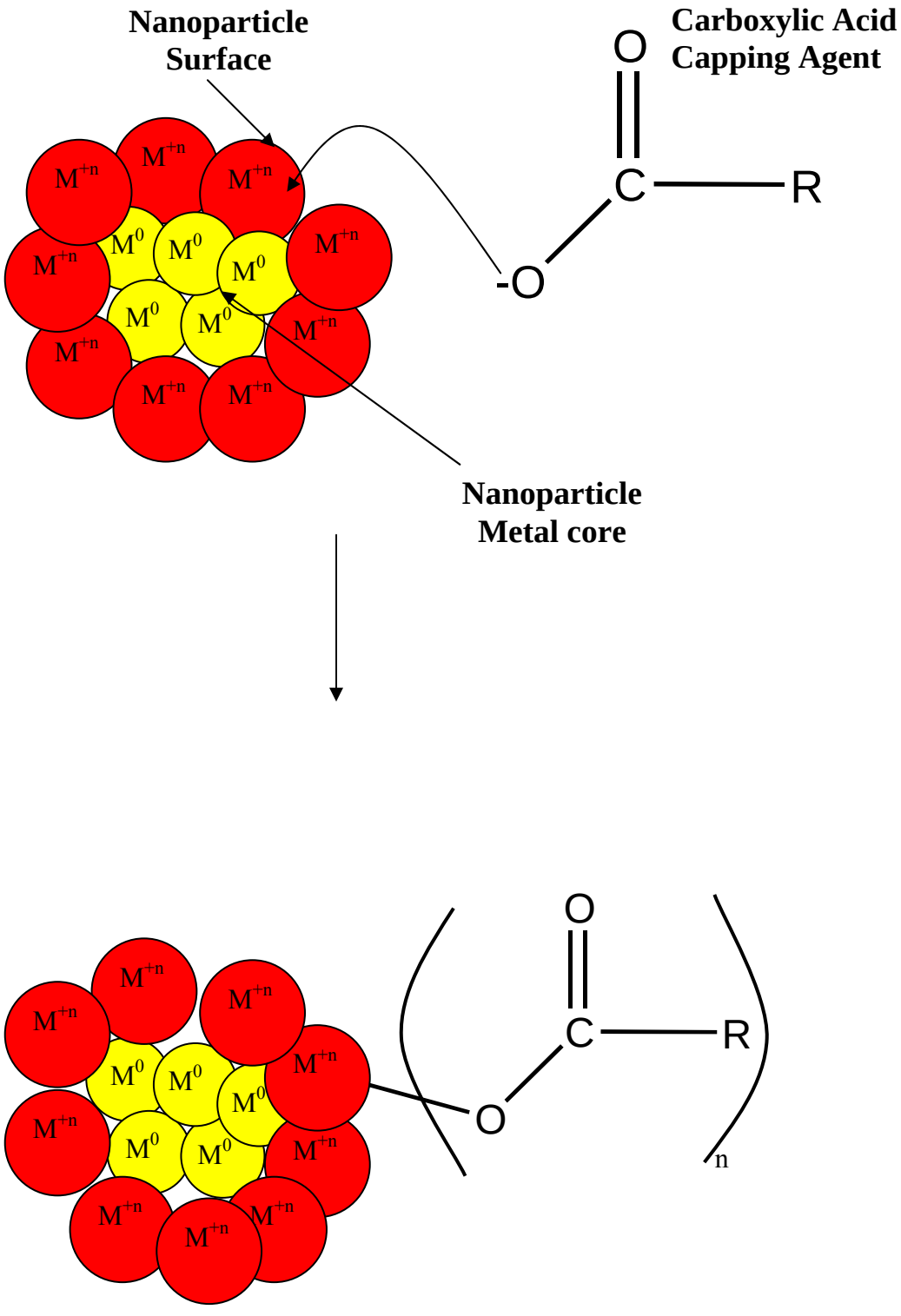


**Scheme 1.1** Bonding of the organic acid to the nanoparticle surface

### 1.3 The Polyol Method

The polyol method was developed in the 1980s, by Fievet et al., for the preparation of finely divided metal powders of easily reducible metals.[13] The method involves reduction of a metal salt with a diol, typically ethylene glycol, diethylene glycol, or a mixture of both.[14] Tetraethylene glycol has also been used extensively. A simultaneous reduction of the metal species and oxidation of the polyol solvent occur.[15] The diol acts as the reducing agent as well as the solvent for the reaction.

One advantage of using ethylene glycol is its reducing power.[16] The reducing power of ethylene glycol has been investigated by analyzing the volatile compounds produced from its oxidation.[14] It has been shown that the reducing action of ethylene glycol is not the same for all metals.[14] For example, Ni metal particles have been prepared from $Ni(OH)_2$ at the boiling point of ethylene glycol, whereas Pd particles can be prepared from $Pd(NO_3)_2$ at room temperature.[15]

One of the least understood aspects of the polyol method is the electrochemistry involved. Linear sweep voltammetry has been used to study the electrochemical behavior of ethylene glycol, and to determine the reduction potential of different transition metals in it at room temperature.[15] The electrochemical window of ethylene glycol (0.4 M $LiNO_3$) was found to lie between –0.82 and 2 V for a Pt electrode, and between –1.15 and 1.65 V for a glassy carbon electrode.[15] The slight differences in these domains indicate different kinetics for oxidation and reduction based on the nature of the electrode.[15] According to Bonet et al., ethylene glycol was observed to oxidize at potentials more positive than those of the metal reduction potentials, however completely reduced metals were produced. This was explained by the fact that the measured potentials are the sum of

the thermodynamic potential and overpotential. They found that the potential becomes more negative as the temperature increases.[15]

The metal salt must be soluble in the diol, so the metal acetate or acetylacetonate is generally used. Even the less soluble hydroxide and oxide forms of Co, Ni or Cu have been completely reduced.[14]

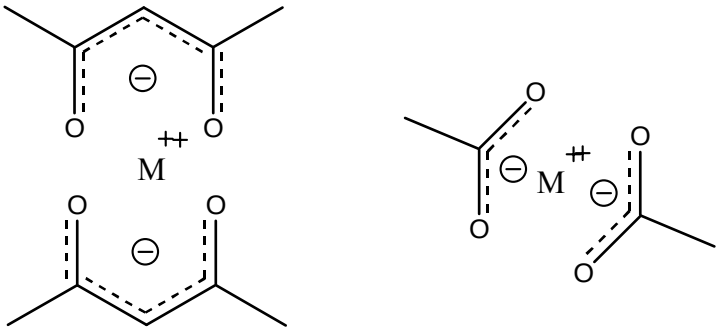


Bis-acetylacetonato M(II) Tetrahedral

Metal (II) acetate

**Figure 1.3** Structures of $M^{+2}$ complexes with acetylacetonate and acetate ligands investigated in the polyol process

The solution is heated until boiling, and a complete reduction of the metal can be achieved within a few hours.[13] The earlier work with this process produced finely divided metal powders with micro scale dimensions. Subsequent work with the polyol process has made it an accepted method for preparing nano scale materials. The polyol process has also been extended to include the use of thiols. This variant on the method produces nanowires rather than the spherical nanoparticles produced by the diols.[17] Alloys have also been produced via this method with atomic level mixing.[18]

The polyol mechanism is poorly understood, but it is thought to occur via the ethylene glycol being oxidized to the diacetyl.[15,19,20]

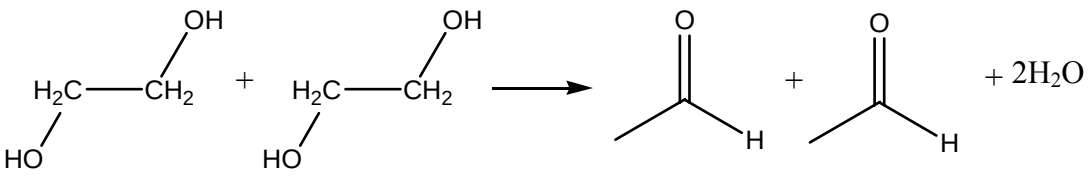


**Reaction (1)**

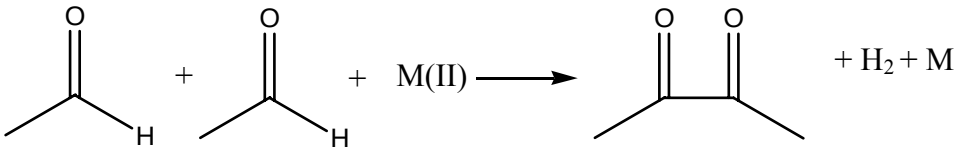


**Reaction (2)**

**Scheme 1.2** Proposed metal reduction mechanism

In the first step of this reaction, the diol is dehydrated to form an aldehyde. The aldehyde is then oxidized twice by the metal salt to form a diketone.[14,21] The reaction is thought to proceed via dissolution rather than solid phase transformation as shown in **Scheme 1.3** .[14] This means that the metals are reacting while solvated as the acetate species. Nucleation and metal nanoparticle growth also occur in this liquid phase. Nucleation and growth must be two completely separate steps in order to keep the particles from agglomerating.[14,22] The first process is the nucleation step. The nanoparticles form in the liquid phase of the supersaturated diol solution. In the second phase of the process, these seed nanoparticles grow into larger nanoparticles and finally fall out of solution as a precipitate.

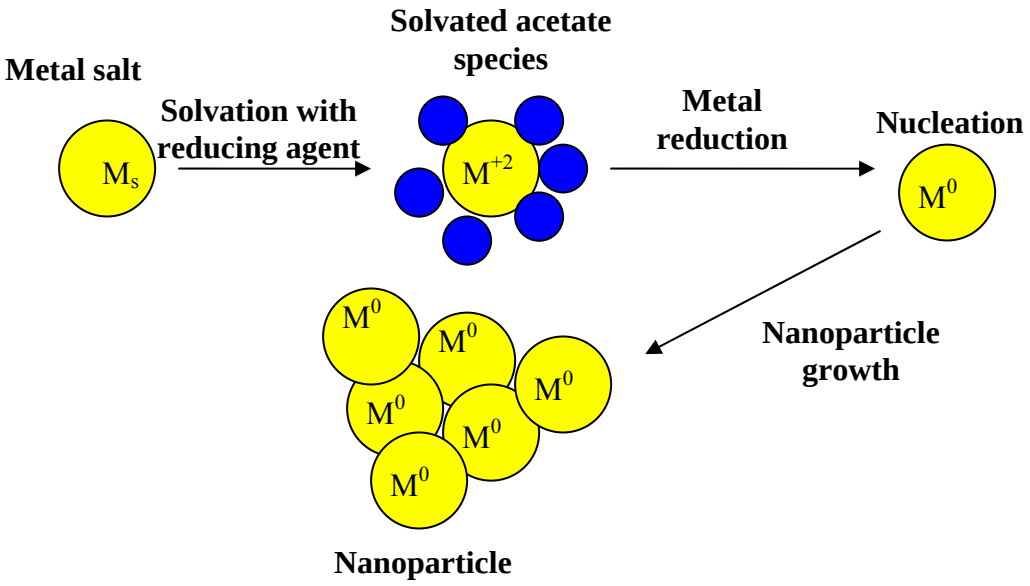


**Scheme 1.3** Mechanism of metal core-shell formation and precipitation from corresponding metal salt $M_s$

After the metal particles form in the polyol solvent, they precipitate out as solid metal nanoparticles. In some variations of the polyol method, this precipitation occurs when the saturation point of the liquid polyol has been reached, which is thought to be very small.[14] There are modified versions of the method in which precipitation of the metal doesn't occur during the reaction because the reaction is carried out in a nonpolar solvent. This nonpolar solvent prevents precipitation because the particles are normally capped with a long chain hydrocarbon. In order to precipitate the particles, ethanol is typically used. From X-ray diffraction and IR spectroscopy, it has been determined that the metal intermediate phases show a lamellar, incompletely ordered structure with intercalation of the solvent/reducing agent molecules and the corresponding alkoxy radicals. These intermediate phase structures, along with the final particle structures, differ from metal to metal.[14]

Temperature plays a big role in the reaction because it influences the rate of reaction by controlling diffusion of the intermediate phase of the metal and likewise the reduction of the metal. Temperature also influences the reduction potential of the ethylene glycol along with the breaking and formation of chemical bonds.[23] The standard reduction potentials of some common metals not bound by a particular ligand are listed in **Table 1.1**. Ligands do affect the standard reduction potentials of metals. The polyol method reduces metals bound by ligands such as acetate and acetylacetonate. It is generally accepted that ligands contribute to a negative shift in the standard redox potentials of metals because the ligand binding inhibits electron transfer to the metal center.[24]

| Reduction | Potential (E°) |
|---|---|
| $Co^{+2} \longrightarrow Co^{0}$ | –0.28 V |
| $Fe^{+2} \longrightarrow Fe^{0}$ | –0.447 V |
| $Fe^{+3} \longrightarrow Fe^{0}$ | –0.037 V |

**Table 1.1** Standard reduction potentials of selected divalent metals

Controlling the size of the nanoparticles is essential, and this is another reason the polyol method works very well for this type of synthesis. In order to produce a uniform size of nanoparticle, it is very important to reduce the occurrence of coagulation of the individual particles. The polyol used in the reaction can help avoid coagulation because, it can be adsorbed and produce steric stabilization which in turn inhibits agglomeration of the particles during growth.[22] After the nuclei have been created in the liquid phase of the solvent the metal crystal growth initiates on these nuclei to form the nanoparticle. As long as the metal is provided slowly by the reduction, the process will produce uniform

sized particles.[14] The metal species is reduced relatively slowly throughout the course of the reaction due to shifts in the equilibrium caused by growth of the metallic phase.

Particle size and shape can be easily directed with the polyol method. Temperature, amount of metal precursor and the application of an external magnetic field (when ferromagnetic metals are used) are just a few factors that govern the polyol reaction and can influence particle size and shape. For instance, if the temperature is increased, the size of the particles normally decreases, as a result of more nuclei being formed in a shorter amount of time, allowing the intermediate metal phase to diffuse more rapidly.[14] When the ratio of metal precursor to polyol is increased, the particle size increases due to the fact that the number of nuclei formed during the nucleation step at a certain temperature is independent of the amount of metal salt introduced to the system. If the number of particles is constant, but more metal is available, the particle sizes will increase.[14]

Another reason the polyol method works well for synthesizing nanoparticles is because it is not as susceptible to impurities as are other methods. The level of impurities in the metal precursor hydroxide form of cobalt, $Co(OH)_2$ , such as Ca, Fe, or Na, have been found to be much lower compared to a solid-gas reduction which relies on the chemical removal of oxygen from an oxide. In part, this may be due to the polyol's relative inability to reduce these to the pure metals. For example, Ca and Na contaminants were reduced by almost two orders of magnitude using the polyol method verses solid-gas reduction.[14] However, a significant draw back associated with the polyol method is the possibility of the final product containing a noteworthy weight percent of

carbon which results from the reaction taking place in the liquid phase in the polyol solvent.[14]

### 1.4 Microwave Overview

Electromagnetic waves contain both magnetic and electric field components. The electric constituent applies a force on charged particles causing them to move within the electric field. The more rapidly the particles move, the more the particles become polarized. At the molecular level, polarization involves distortion of the electron cloud surrounding a molecule or physical rotation of molecular dipoles.[25] Microwaves are electromagnetic waves. Most commercial laboratory microwaves use a 2.45 GHz frequency corresponding to a 12.2 cm wavelength range, between infrared and radiowave wavelengths.[23] The forces in these waves change direction at a rate of approximately 2.4 x $10^9$ times per second.[23] Most material exposed to microwaves can not respond fast enough to these changes in wave direction which induces friction, which, in turn, produces heat.

In order for the microwaves to be effective heat sources, the material that the microwaves are being applied to must be able to couple with the microwave energy. In other words, the material should be able to efficiently convert electromagnetic energy into heat at a given frequency and temperature. This is known as the dielectric loss constant ε".[23] A dielectric material is one which allows charge to be stored and no dc conductivity is observed between plates.[25] A dielectric material would act as a capacitor when placed between two electrodes. The heating rate dependence on the presence of a dielectric field is:

$$\text{Tan } \delta = \varepsilon'/\varepsilon'' \text{ (23)} \qquad \textbf{(1.1)}$$

Where ε' is the measure of the molecule's ability to be polarized in an electric field.[23] The dielectric heating rates rely on Tan δ, which itself is dependent on frequency, temperature, physical state and composition.[23]

The volume of the material and the geometry of the microwave cavity and the reaction vessel exposed to the microwaves are all important factors in heating rate. Tan δ is related to penetration depth by:

$$D_p = \lambda_o \sqrt{\varepsilon' / \varepsilon''}\ ^{(23)} \qquad \textbf{(1.2)}$$

If the volume is increased, the waves experience an absorbance loss. $D_p$ is the penetration depth of the incident waves and $\lambda_o$ is the wavelength of the microwave.[23] 2.45 GHz is the frequency most often used because of its penetration depth in most laboratory samples.[26] Because the microwave field is not homogeneous in the sample, uneven field distribution can have an effect on chemical reactions taking place in the microwave. This inconsistency in the energy can lead to hot spots in the sample if the energy generation is faster than heat transfers.[27] These hot spots lead to the unusual temperature profiles witnessed in microwave heating.

### 1.4.1 Laboratory Use of Microwaves:

When compared to thermal heating, microwave heating has many benefits in organic synthesis, such as rapid volumetric heating, higher reaction rates, higher reaction selectivity, higher product yield and energy saving.[28] In conventional thermal heating, heat transfers depend on the thermal conductivity, temperature difference across the materials and convection currents.[27] Microwave heating removes all these variables because in microwave heating, the energy source of the microwaves are not in direct

contact with the reaction solution, so the heat produced is via dielectric heating. This can lead to completely different temperature profiles.[25]

One factor that plays a role in microwave heating is superheating in the presence of a large number of ions.[23] Electrolytes affect the ability of the material to couple with microwaves efficiently. Electrolytes generally have a large dipole moment which allows them to convert microwave energy to heat better than less polar molecules. When the solvent component of a reaction mixture is able to efficiently couple with the microwave energy, the heating rate is dramatically increased. This type of heating is not really any different than thermal heating, because with thermal heating, the solvent is being heated and in-turn heating the reactants. The only difference would be the rate at which the reaction was brought up to temperature; this leads to reduced energy consumption. If a non-polar solvent is used for the reaction, and the reactants dissolved in the solvent are able to couple with the microwave energy effectively (i.e. they are good electrolytes), the heating is markedly different from thermal heating. When the reactants themselves are absorbing the microwave energy, heating becomes even faster and more efficient.[23] It would be ideal to use a solvent that has a low dielectric loss and use reactants that have high dielectric loss constants.

The use of nonpolar solvents can affect the reaction mechanism because, when using microwave heating, there would be less coupling of the microwave energy with the solvent. This would allow the reactants to absorb the microwave energy and transfer the energy to the solvent instead of the solvent transferring the energy to the metal salt being reduced, similar to traditional thermal heating. It has been shown that the magnitude of the perceived microwave effects decreases with increasing solvent polarity.[29]

Conventionally, organic synthesis has been carried out under conductive heating conditions. The reaction vessel is placed in contact with the heat source, and the materials inside are heated through convection. This is an inefficient way to transfer heat because it depends on the thermal conductivity of the glassware and the solvent.[26] Microwaves penetrate the glass surface of reaction vessels. The glassware does not interact with the microwaves and therefore does not undergo dielectric heating, and most organic solvents used have large $D_p$ values. Therefore, the maximum temperature of the reaction mixture can be achieved within the entire reaction vessel as opposed to just the outer portion with conventional heating. This has been confirmed using IR imaging.[30] This dielectric heating can produce different temperature profiles during the reaction and can lead to different chemical product distributions from the reaction.[25] These differences in product yields may be due to the possibility that certain isomers produced during thermal heating may not be stable under microwave super heating, and therefore a different isomer ratio is observed.[30]

During microwave heating, if there is inefficient mixing of the solution, boundary effects can have an impact on the reaction progress. This is another reason for the different temperature profiles observed during microwave reactions as opposed to thermal heating reactions. A phenomenon known as nucleate boiling occurs at the surface of a reaction vessel and its rate is governed by the temperatures at the surface and availability of nucleation sites.[30] Nucleate boiling is not observed in microwave reactions. During a microwave reaction, the temperature at the surface of the reaction vessel is lower than the internal temperature, therefore a steady state boiling point is achieved at a higher temperature.[30] The higher steady state boiling points observed in the microwave

reactions are influenced by the wetting properties of the solvent, the power input, surface condition and surface tension.[30] It has been shown that organic solvents can superheat by 13-26 °C above the normal boiling point at atmospheric pressure which indicates the importance of the wetting properties of the solvent.[23] These different temperature zones can lead to control of kinetic vs. thermodynamic isometric ratios of the products.[23]

**1.4.2 Specific Microwave Effects:**

There have been debates for years over the question of microwaves causing chemistry that is unique only to microwave energy. The overwhelming evidence points to the fact that there are no known unique microwave effects. Most rate enhancement effects that have been reported are simply due to poor temperature control and monitoring.[23] A more detailed survey of microwave reactions revealed that they are governed by the same fundamental principles of thermodynamics and kinetics as reactions using thermal heat sources.[25] The region of electromagnetic energy that microwaves operate in can only affect molecular rotation, not its structure.[26] Microwaves contain about $2.39 \times 10^{-4}$ kcal/mol of photons.[23] The energy contained in these photons is very low when compared with the energy to cleave a molecular bond which is typically 80-120 kcal/mol.[26] It is safe to assume that microwaves will not affect the molecular structure of materials within the reaction vessel. Therefore no unique chemistry should be attributed solely to microwaves themselves. Molecular activation such as that in photochemistry could only be achieved by the species in solution somehow storing the microwave energy and giving rise to an activated state. The microwave energy would either have to be stored in the vibrational energy of the molecule by e.g. an antenna group or by alignment of molecules.[23] This activated state could only be achieved through a step-by-step

accumulation of energy from the microwaves. This possibility can be ruled out because of a fast relaxation time.[27]

It is easy to understand why microwave effects have been credited with rate enhancements. Because steady state boiling is achieved during microwave heating, the reaction proceeds at a much higher temperature than it would with conductive heating. A superheating effect of $30^0$C leads to a rate enhancement of about 8 fold.[30] There is also a significant reduction in the time it takes to reach the steady state boiling temperature using microwaves. A 10-50 fold reduction in time could be achieved using microwave versus conventional heating.[30] Only reaction rates that are enhanced by 100-1000 fold at atmospheric temperatures can be attributed to microwave effects.[30]

Rate enhancements when using microwave energy have been reported for a number of organic syntheses. These accelerated reactions are a result of material-wave interactions, which lead to thermal effects.[29] Any type of specific microwave effect can always be explained by a more conventional thermal effect. When reactions have been carried out under carefully monitored reaction conditions, no specific microwave effects have been found, but an accurate comparison to thermal heating is difficult to attain.[27]

**1.5 Microwave Polyol**

Komarneni was the first to report metallic powders produced via a microwave polyol method.[31, 32] Microwave synthesis is an optimal method for preparing nanoparticles via the polyol method. The metallic particles that are produced during the polyol reaction are excellent receptors for microwave energy which leads to even more rapid heating of the solution.[19] When these metallic particles are exposed to microwave radiation it can create localized superheated regions in the solvent. This phenomenon is

known as The Maxwell-Wagner effect, or interfacial polarization.[33] This effect occurs when particles that couple well with the microwaves are in contact with nonconducting materials. These hot spots speed up the reactions between the metal particle and the organic substrate.[25] The localized super heated regions produced could be similar to what is observed in sonochemical methods.[27, 34] Smaller sample sizes or stirring the sample while in the microwave oven can help lessen the effect of these hot spots, but this can lead to other problems.[27] The localized super heated regions make for a more rapid synthesis of organometalic nanoparticles, and also allows for the formation of even smaller nanoparticles. These smaller particles are formed because in the super heated regions, the reaction rate of the organic coating with the metal surface is increased, thus the particle is not allowed to grow very large before it is capped.

Another reason microwave synthesis is an ideal method for the polyol synthesis is because polyol solvents such as ethylene glycol have a large dipole moment.[16] The dielectric constant for ethylene glycol at 25°C is 41.4.[34] This high dielectric constant allows the solvent to couple extremely well with the electromagnetic waves and leads to much faster heating of the solvent. These high boiling point solvents are also well suited for microwave synthesis because they are known to prevent arcing. Arcing is known to cause degradation of solvents in microwave-assisted reactions. The high weight percent of carbon, sometimes associated with the polyol method, can be linked to this arcing phenomenon.[19]

The microwave polyol synthesis has many advantages over the conventional heating polyol synthesis. The localized hot spots created by the microwave synthesis produce much smaller particles than are produced in conventional heating which

normally produces micron sized particles.[13] Under microwave radiation, solvents undergo significant overheating, the consequence of which is that a metal ion can be reduced to its zero oxidation state via the previous proposed mechanism.[31] With conventional heating, only the most easily reducible metals can be converted to metal powders.[13] Microwave heating allows for metals such a $Fe^{+2}$ to be reduced.[35] As discussed before, the microwave heating reduces impurities in the product, and the reaction time is reduced from hours to minutes. One disadvantage of the microwave synthesis is that it tends to produce more agglomerated particles than some other methods such as sonochemical.[19]

### 1.6 Magnetite ($Fe_3O_4$) and Cobalt Ferrite ($CoFe_2O_4$)

Magnetite nanoparticles can be readily synthesized via the polyol method. During the reaction of iron salts with a 1,2 diol, air can be sparged through the reaction to produce magnetite nanoparticles.

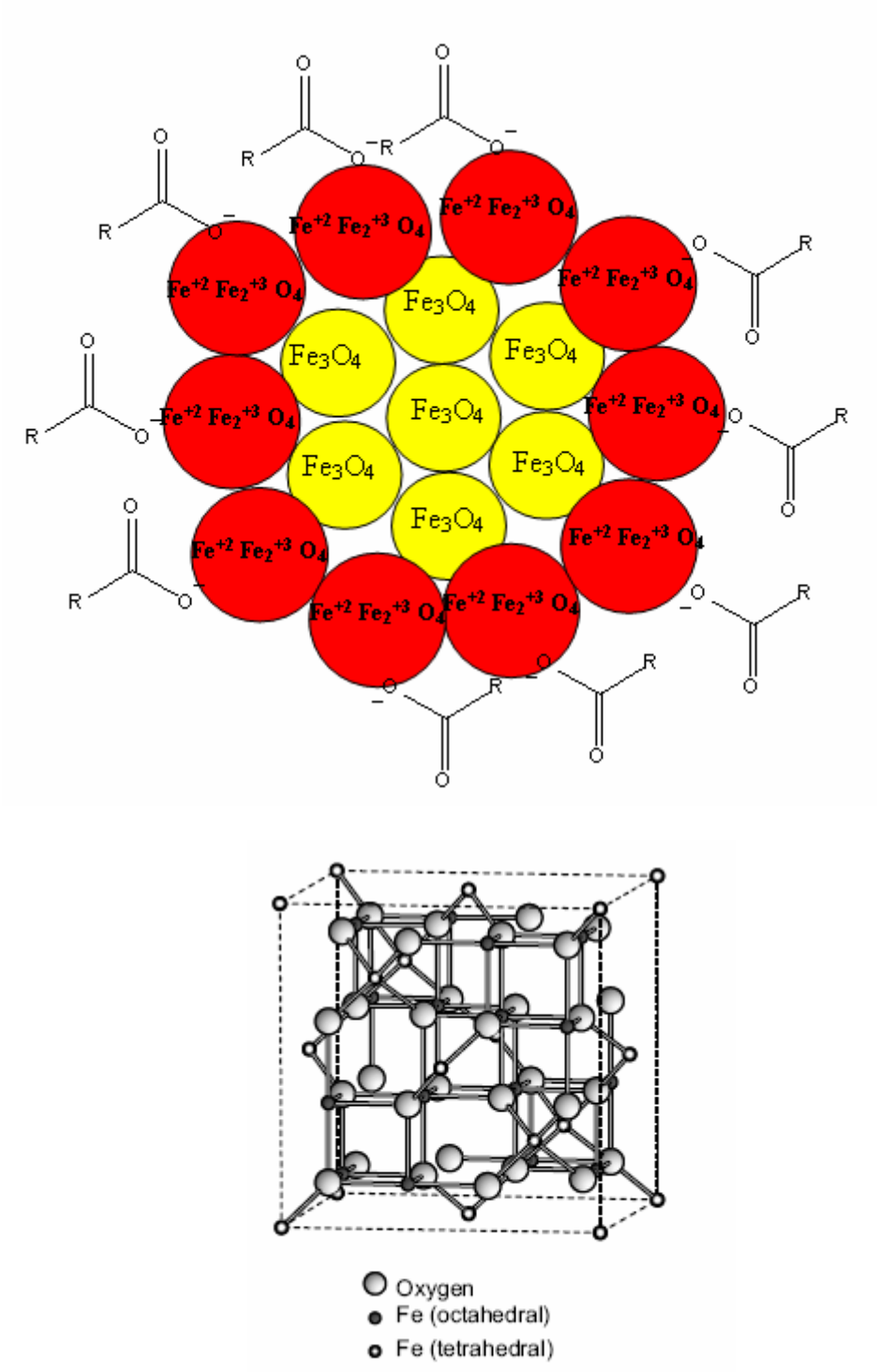


**Figure 1.4** Schematic of magnetite core-shell nanoparticle (top) and crystal lattice structure of magnetite[36] (bottom)

Magnetite is a fairly common iron oxide. It is a member of the spinel group, which has the general formula $AB_2O_4$. In magnetite A is $Fe^{+2}$ and B is $Fe^{+3}$.[37] Oxygen forms a fcc closed packing and the Fe cations occupy the interstitial tetrahedral sites and octahedral sites.[38,39] The tetrahedral sites contain Fe(III) and the octahedral sites contain both Fe(II) and Fe(III).[40] These octahedral sites contribute to magnetite's interesting properties, because the electrons can flow between the $Fe^{+2}$ and $Fe^{+3}$ ions in these sites at room temperature.[38] This transfer of electrons creates an electric vector which generates a magnetic field.[37]

Ferrite nanoparticles are of great interest in the scientific community because of their potential application in ferrofluids, magnetic fluids, magnetic recording media, and magnetic resonance imaging.[41, 42] Magnetite particles can also be coated to aid in clinical medicine.[38] The crystallinity of magnetite nanoparticles can strongly affect their magnetic properties, therefore it is very important to be able to produce high quality magnetite nanoparticles.[7] Most of the intriguing and beneficial properties that magnetite possesses are only accessible if the particles are on the 20 nm range, because at this size they can have superparamagnetic properties.[38] This superparamagnetic behavior arises from the infinitely small coercivity brought on by the negligible energy barrier in the hysteresis of the magnetization loop of the particles as predicted by Cloch and Neel.[41] The term "superparamagnetic" means that these particles are attracted to a magnetic field, but when removed from the field, they retain no residual magnetism.[43] This means that these particles can be introduced to a magnetic field without agglomerating once the field is removed, and this can be advantageous in drug delivery.

Through variation of the divalent cations contained in ferrite molecules, their magnetic properties can be finely tuned. Cobalt ferrite particles have been studied extensively because of their ferromagnetic properties.[44] Due to different strengths of magnetic interactions at lattice sites, $CoFe_2O_4$ nanoparticles possess very different magnetic properties than magnetite.[45] The differences in magnetic properties between magnetite and cobalt ferrite have been attributed to the spin-orbital couplings at the $Co^{+2}$ and $Fe^{+2}$ sites in the crystal lattice.[45] $CoFe_2O_4$ nanoparticles have been shown to display much better magnetic characteristics than $Fe_3O_4$.

Our research group is developing highly reactive core-shell nanoparticles that can alter the thermal stability of jet fuel via targeted chemical reactions. At the center of the nanoparticles that are being created is an iron core. The iron core has a zero charge. It is completely reduced and therefore highly reactive to oxygen. This iron core cannot be exposed to the atmosphere therefore it must be protected. During the reaction to form the nanoparticles, oleic acid is added which serves as a surfactant and a capping agent. The capping agent helps to control the particle size and shape, as well as increasing its stability and solubility in organic media. This amphiphilic coating can be taken advantage of as a delivery mechanism for the iron into the hydrocarbon rich environment of jet fuel.

Jet fuel acts as a coolant for the heat generated by the aircraft engine. The temperature of the fuel begins to rise as more heat is transferred to it from the engine. Once the fuel reaches a certain temperature, which has yet to be determined, it is believed that the oleic acid can become permeable to the dissolved oxygen in solution. The ability of $Fe^0$ nanoparticles to remove dissolved oxygen has been investigated by studying the lifetime of pyrene in a hexane solution. The long lifetimes of pyrene above ~$110^0$C

indicate that the oleic acid capped $Fe^0$ nanoparticles did remove the dissolved oxygen present when heated.[46] Once the iron core is exposed, it can immediately react with any dissolved oxygen making it unavailable to undergo the harmful chain reactions leading to harmful deposits.

$$4\ Fe^0 + 3\ O_2 \rightarrow 2\ Fe_2O_3 \quad E°=1.67\ V \quad \textbf{(1.3)}$$

After the iron core reacts with the dissolved oxygen in the fuel, it forms iron oxide or rust. These particulates are also not beneficial to the fuel, so in order to work, there has to be a way of removing them effectively. The removal of these particulates is another area of study for these nanomaterials involving magnetic core-shell nanoparticles. Cobalt ferrite core-shell nanoparticles are being studied to be used as a possible filter to magnetically remove these leftover rust particles.

The polyol method was chosen for this research because it employs relatively mild conditions, softer chemistry and lower temperatures than many other methods such as sonochemical or micellular.[19] The polyol method only requires the solvent be brought to its boiling point, not superheated. Other than the advantage of energy conservation and safety, the preparation of new phases that are inaccessible at higher temperatures because of thermodynamic instability are possible.[19] The starting materials used are also much less toxic than other techniques which use iron precursors such as $Fe(CO)_5$ which releases CO.

# II. EXPERIMENTAL PROCEDURES

## 2.1. X-Ray Powder Diffraction (XRD)

During the course of this research, powder XRD was used to determine the different phases of iron present in the products of each experiment. It was used for compositional analysis and as a probe into the structure of the product. XRD has been widely used for investigating the structural properties of crystals, amorphous samples and layered systems.[47] By comparing the position of the peaks in the diffracted beam to the standards provided by the International Center for Diffraction Data (ICDD), the unknown phases present in each sample can be identified.[48]

After the phase of the material was determined, the XRD patterns were then used to investigate the structural nature of the material, for example, the size and crystallinity of the particles. A material's structure can be either crystalline or amorphous. Crystalline materials have sharp peaks in their XRD patterns while amorphous materials have more diffuse peaks because of fluctuations in the lattice parameters. When it comes to amorphous nanomaterials, smaller sized particles also produce broader peaks in the XRD patterns, however, based on peak width, XRD patterns can be used to estimate size in nanomaterials The peaks are broader for smaller sized nanoparticles even if the particle is highly crystalline because, as the particle size decreases, the crystal lattice becomes less aligned, leading to broadening of the XRD pattern.

The XRD analysis in this work was performed on a Bruker AXS D8 Advance diffractometer equipped with a type KFL Cu 2K source with a 1.54 Å wavelength and a Sol-X detector. Powdered samples were pulverized with a mortar and pestle and placed on a 50 mm zero background silicon single crystal sample holder and pressed into a thin layer using a Fisherbrand Pre-Cleaned Microscope Slide. The sample holder was then placed in the D8 Advance for XRD analysis. The more wax-like samples were smeared onto the sample holder using a cotton swab wetted with a drop of *n*-hexane until a thick enough layer was deposited.

To ensure a clean, complete fingerprint, spectra were obtained in continuous scan mode over a 2θ range of 5° to 85°, with a speed of 5 sec/step, and a diffracted angle increment of 0.05°. A continuous scan option, in which the X-ray source and the X-ray detector continuously repeat the 2θ range, was used on all scans to provide further refining of the X-ray data points. Upon completion of the X-ray sample run, the data were analyzed in the EVA program, which has a built-in diffraction pattern library to compare the sample's diffraction pattern to the diffraction patterns in the ICDD database.

**2.2 Transmission Electron Microscopy (TEM)**

Transmission Electron Microscopy (TEM) was used in this work to determine the size, shape and arrangement of the particles produced from some of the reactions. The TEM analysis done for this work was performed by the Materials and Manufacturing Lab at the Air Force Research Lab by Pam Lloyd and Lt Melissa Ingram and by Dr. Sun's group at Clemson University. To obtain TEM images, a Hitachi HD2000 STEM system was used. The solid samples were dispersed in a chloroform solution using a sonocating bath. The samples were transferred onto custom carbon-coated 300 mesh copper grids for

TEM imaging. The use of carbon-coated grids ensures that the background will be of low density and have little contrast in the TEM image.

When analyzing a TEM image, both light and dark areas will be visible. The lighter areas are areas where the material is less dense and more electrons have passed through. The darker areas are where the material has greater electron density and fewer electrons have been transmitted through. The material the electrons are passing through in this work is both the organic coating as well as the core nanoparticle. This light and dark contrast can be reversed if the instrument is in the Z-contrast mode. Because inorganic particles, such as iron oxides, tend to be dense agglomerations of atoms with relatively higher atomic weights than organic materials, they will impede the flow of electrons through the sample. The less dense areas of the material, such as the organic coating, will allow more electrons to penetrate; therefore we should only see the iron oxide core on a TEM image. From the TEM images, one can determine the size, shape and arrangement of the inorganic particles in the sample.

### 2.3 Atomic Force Microscopy (AFM)

AFM images obtained in this work were done on a multimode Nanoscope IIIA Microscope, manufactured by Digital Instruments Veeco Metrology Group. The AFM was operated in Tapping Mode using an N-type phosphorus-doped silicone tip. The diameter of the tip was between 10-20 nm. AFM specimens were prepared by drip coating a 1mg/mL sample solution onto small silicone wafer chips followed by drying in air.

## 2.4 Fourier Transform Infrared (FT-IR) Spectroscopy

The FT-IR spectrometer used in this work was a Perkin Elmer System 2000 FT-IR. To prepare the powdered samples for analysis, a small quantity of purified KBr was added to the pulverized powdered sample and pressed into a pellet. The waxy samples were prepared for analysis by smearing a thin layer on KBr salt plates with a cotton swab moistened with *n*-hexane. The sample chamber was purged with nitrogen during analysis for all samples unless otherwise noted. Each spectrum consisted of 16 scans with 1.0 $cm^{-1}$ resolution.

## 2.5 Thermal Polyol Core-shell Nanoparticle Synthesis

Attempts were made to reproduce the results of a published iron oxide core-shell nanoparticle synthesis.[33, 49] From the literature, the process was adapted slightly from two different papers. All reagents were purchased from Sigma Aldrich and used without any further purification. The amounts of reagents used were roughly the following ratios unless otherwise noted: 1 mmol of the iron source (254 mg iron (II) acetylacetonate) to 2 mmol of the reducing agent (517 mg 1,2-hexadecanediol); 1 mmol of capping agent (320 μL oleic acid); 20 mL of solvent. The oleylamine used in published reports was left out because the literature indicated that it was only used because it bound to the Pt more readily than the oleic acid, and the goal of the experiment was to create Fe nanoparticles, not FePt nanoparticles.[36]

The reagents were added to a two neck round bottom flask. To ensure proper mixing of reagents, samples were placed in a Solid State/Ultrasonic FS-28 Sonocating Bath for approximately 30 min. The brownish yellow liquid was placed in a heating manifold with a condenser attached. The heating manifold was turned on and the liquid

reached approximately 280°C, and it remained at that temperature for 30 min. Air was sparged through the reaction flask throughout the reaction to promote the formation of magnetite particles. Small gaseous emissions were noted during the reaction which decreased the temperature almost 10°C every emission. It isn't clear what caused these emissions. The flask was removed from the heat and allowed to cool. The black liquid was then separated into two vials and approximately 20 mL of ethanol was added to each vial to precipitate the product.

It was apparent that a precipitate began to form immediately, as the solutions became opaque and cloudy. The vials were then left to sit over night. The precipitates were a dark brown color and the supernatant was a clear, pale brown. Products were centrifuged in an Eppendorf Centrifuge 5804 counter balanced with a centrifuge tube containing DI water. The solutions were typically centrifuged for 30 minutes at 5000 rpm for every wash step. Washes consisted of sonicating in ethanol three times and a final sonication in *n*-hexane. The solution fractions were typically discarded after centrifuging leaving a brown powder insoluble in both ethanol and *n*-hexane. The product was dried under a nitrogen flow.

After successful synthesis of magnetite nanoparticles, the same procedure was used to synthesize $Fe^0$ nanoparticles. In-order to produce $Fe^0$ particles, oxygen had to be removed, thus the reaction mixture was sparged with nitrogen for 30 min prior to heating. Nitrogen was sparged through the vessel through out the reaction. The resulting solid was a dark brown wax. These products were washed and centrifuged as in the previous procedure, but these products were soluble in *n*-hexane. The product was dried under a

nitrogen flow. This procedure was repeated using microwave heating. The products from each heat source were compared.

**2.6 Microwave Polyol Core-shell Nanoparticle Synthesis**

The procedures for the microwave reactions were adapted from the thermal polyol reactions. The amounts of reagents used were roughly the following ratios unless otherwise noted: 1 mmol of the iron source (254 mg iron (II) acetylacetonate, or 174 mg iron (II) acetate ) to 2 mmol of the reducing agent ( 517 mg 1,2-hexadecanediol or 20 mL of liquid polyol solvent); 1 mmol of capping agent (320 μL oleic acid); 20 mL of solvent. However, neither the Pt co-reactant nor the oleylamine co-capping agent reported in the literature were used unless otherwise noted. The reagents were added to a round bottom flask. To ensure proper mixing of reagents, samples were placed in a Solid State/Ultrasonic FS-28 Sonocating Bath for approximately 30 min. The brownish yellow liquid was placed in a CEM Discover Microwave Synthesis Workstation equipped with a condenser column with a nitrogen line fed through it. The reaction mixture was sparged with nitrogen for 30 min prior to turning on the microwave. A stir bar was also added to the flask and the stir plate on the microwave was turned on. The temperature was set at 270°C. Depending on the solvent/reducing agent used, the temperature did not always reach 270°C in the course of the reaction. The temperature was controlled automatically through power adjustment. The maximum power (300W) was applied to the microwave cavity until the set temperature was reached. Nitrogen was sparged during the reaction (air was never used for the microwave reactions).

Once the set time in the microwave had elapsed, the flask was removed from the microwave and allowed to cool. The liquid was then separated into two vials and

approximately 20 mL of ethanol was added to each vial to precipitate the product and left to sit over night. Products were centrifuged in an Eppendorf Centrifuge 5804 counter balanced with a centrifuge tube containing DI water. The solutions were typically centrifuged for 30 minutes at 5000 rpm for every wash step. Washes consisted of sonicating in ethanol 3 times and a final sonication in *n*-hexane. The ethanol solution fractions were discarded after centrifuging leaving a black wax soluble in *n*-hexane. The product was dried under a nitrogen flow. All variations to these procedures have been summarized in **Tables 3.1 – 3.12**.

The application of microwave energy involving metal powders seems to have obvious drawbacks, but it has been shown that this synthetic procedure can be performed safely and successfully.[50] One possible problem with producing metal nanoparticles in a microwave is the possibility of arcing. This arching can cause a degradation of the solvent and lead to high levels of carbon in the resulting products. Mingos and Whittaker have shown that the used of high boiling point alcohols in microwave reactions can prevent this arcing.[50] Alcohols seem to prevent arcing because of their significant dielectric loss tangent. This large loss tangent leads to a decrease in electric field strength and thus induced voltages in the metal.[50]

# III. RESULTS AND DISSCUSSION

## 3.1 Research Overview

The main purpose of this research was to produce different types of iron and cobalt core-shell nanoparticles capped with oleic acid (along with other possible capping agents) via thermal and microwave polyol methods. One of the main parameters that was changed during the course of the investigation into the thermal polyol and microwave polyol processes was the choice of solvent/reducing agent. The microwave polyol solvent was changed during the course of this exploration from a non-polar ether to a relatively polar 1,2-hexanediol. The change was made to examine the difference between the three types of heating: 1) conventional thermal heating 2) microwave heating with a non-polar solvent 3) microwave heating with a polar solvent (which should mimic the products of conventional thermal heating). The following scheme represents our proposed polyol mechanisms, based on the literature,[15,19,20] for the 1,2 diols and divalent metals investigated.

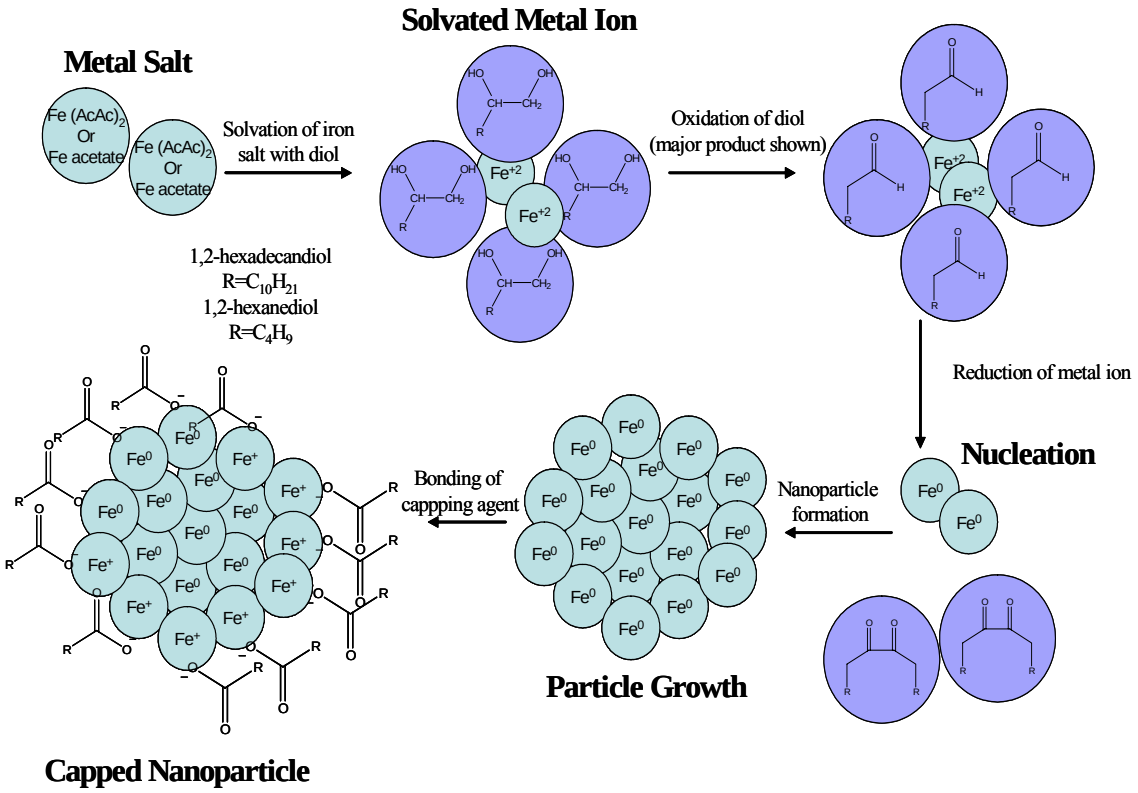


**Scheme 3.1** Proposed metal reduction mechanism for diols and metals investigated

In the first step of this scheme the iron salt is solvated by the respective diol (either 1,2-hexadecanediol or 1,2-hexanediol). The diol is then oxidized, and two possible oxidation products are possible. The predicted major product is illustrated in **Scheme 3.1.** This would be the major oxidation product because it would have the more stable enol form than the other possible aldehyde. This oxidation product then reduces the metal and is oxidized to the diketone. Once the metal is produced, more metal grows on these nucleates and then forms metal nanoparticles. These metal particles are formed in the presence of surfactants, which cap the nanoparticle thus stopping any further growth.

### 3.2 Thermal Polyol Magnetite Core-shell Nanoparticle Synthesis

The first set of experiments was conducted to reproduce published results of nanoscale magnetite particle synthesis under conventional thermal heating conditions.[33,49] These conditions are summarized in **Table 3.1**

| Sample # | Type | Capping Agent | Reducing Agent | Solvent | Metal Salt | Variation |
|---|---|---|---|---|---|---|
| **1** | Fe w/ $O_2$ | oleic acid | 1,2-hexadecanediol | octyl ether | Fe $(Acac)_2$ | |
| **2** | Fe w/ $O_2$ | oleic acid | 1,2-hexadecanediol | octyl ether | Fe $(Acac)_2$ | reduction by ¼ |
| **3** | Fe w/ $O_2$ | oleic acid | 1,2-hexadecanediol | octyl ether | Fe $(Acac)_2$ | solution fraction investigated |
| **4** | Fe w/ $O_2$ | oleic acid | 1,2-hexadecanediol | octyl ether | Fe $(Acac)_2$ | Repeat of #1,2 and 3 |

**Table 3.1** Summary of thermal polyol magnetite syntheses reagents and conditions

The first reaction, using thermal heating, produced a brown powdered product. FT-IR was performed to identify the characteristic features that are associated with capped nanoparticles. **Figure 3.1** shows the FT-IR spectra of the product from the magnetite core-shell nanoparticle synthesis and oleic acid, respectively. The $\nu$(C=O) stretch at 1710 $cm^{-1}$ in the oleic acid spectrum is not present in the FT-IR spectrum of the magnetite product, this is common to all acids used to cap nanoparticles.[29] The FT-IR spectrum of the product shows the two signature bands at 1600 $cm^{-1}$ and 1480 $cm^{-1}$ that correspond to the $\nu_s$(C=O) and $\nu_a$(C=O) stretching modes and indicate that the oleic acid bonded to the surface of the metal particle. It has been suggested that surfactants such as oleic acid bond to the surface of iron oxide nanoparticles via ionic bonds, in other words, as the oleate species.[12] All other bands below 2000 $cm^{-1}$ are due to the $\nu$(C-C) stretch, $\nu$(C-O) stretches, $CH_2$ deformations and other motions that are too complex to assign[51,52]

and match those from the oleic acid spectrum, indicating the oleic acid chain is still present.

The IR bands in the 2850-2960 $cm^{-1}$ region arise from the $CH_2$ symmetric and asymmetric stretching, respectively,[12,29,52] of the oleic acid carbon chain. The small band at 3003 $cm^{-1}$ is due to the *v*(C-H) mode of the C-H bond adjacent to the C=C bond of the oleic acid, and the very small peak at around 1650 $cm^{-1}$ is from this *v*(C=C) mode.[52] A broad *v*(O-H) stretch at 3400 $cm^{-1}$ is present as well. This is attributed to hydrogen-bonded hydroxyl groups.[51,53] The *v*(O-H) stretch in the FT-IR spectrum of the magnetite product at 3400$cm^{-1}$ is more pronounced than in the oleic acid FT-IR. This feature is very common in the FT-IR spectra acquired on polyol products. The two bands at 2400 $cm^{-1}$ and 2390 $cm^{-1}$ are from $CO_2$ because the chamber was not purged with nitrogen prior to acquiring the spectrum.

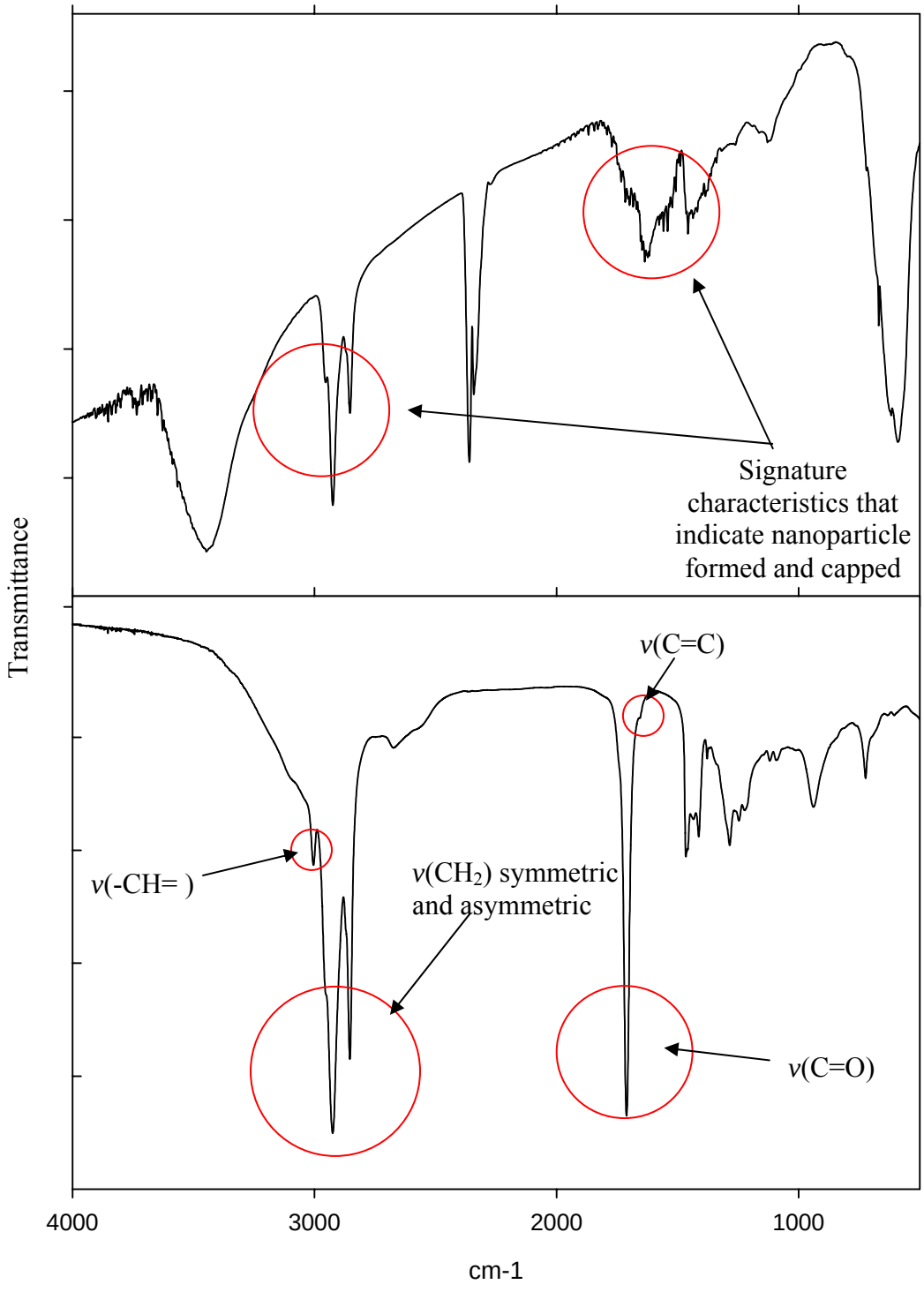


**Figure 3.1** FT-IR spectrum from thermal magnetite core-shell nanoparticle product (top) and of oleic acid alone (bottom)

The XRD pattern shown in **Figure 3.2** displays a well resolved magnetite structure based on comparison to the ICDD database. Using the Scherrer equation, particle sizes can be estimated based on the peak width at half the height of a peak in the XRD pattern.[54]

$$t = 0.9\lambda/B\cos\theta \qquad (3.1)$$

Where $\lambda = 1.54$Å, B = broadening of the peak at full width half max, $\theta$ = angle of incidence (Bragg angle) and t = particle size.

Based on this equation, particle sizes were estimated to be about 5 nm. From the FT-IR data, it was determined that the magnetite particles were successfully capped with the oleic acid. All data agreed with published reports. Because magnetite is a naturally occurring magnet, the magnetite products should respond to an external magnet, which was confirmed with a common refrigerator magnet. It was not expected that $Fe^0$ would be produced from this reaction because it was done in an ambient environment. Repeat syntheses were performed, and all results were reproducible.

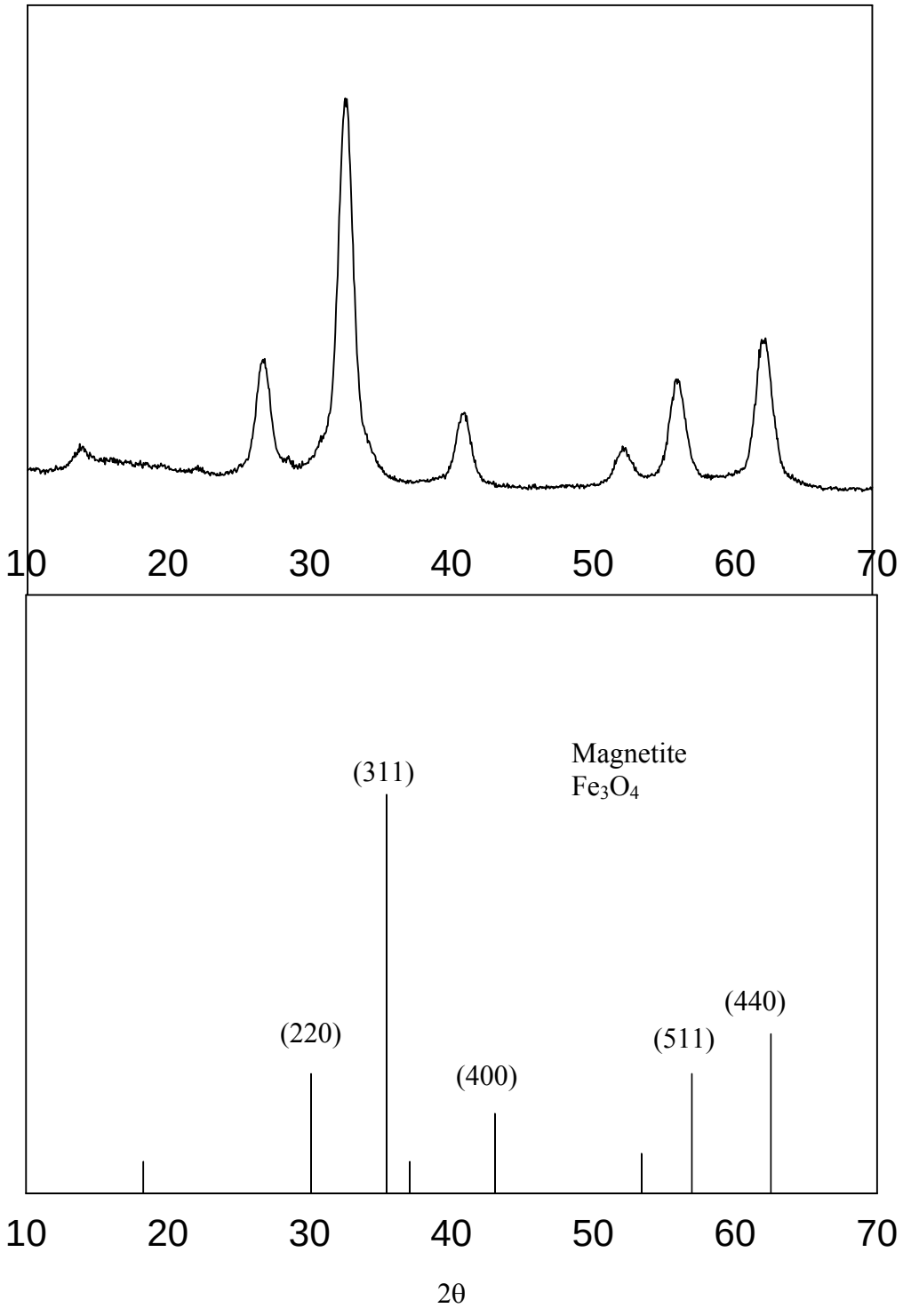


**Figure 3.2** XRD pattern from thermal polyol magnetite core-shell nanoparticle product (top) and ICDD database diffraction pattern of $Fe_3O_4$ with labeled Miller-index planes (bottom)

### 3.3 $Fe^0$ Core-shell Nanoparticle Synthesis Attempts: Thermal and Microwave

After the published results of core-shell magnetite nanoparticles had been repeated, and reproducibility established, syntheses of $Fe^0$ core-shell nanoparticle were attempted. **Table 3.2** summarizes reaction conditions for these reactions.

| Sample # | Type | Capping Agent | Reducing Agent | Solvent | Metal Salt | Variation |
|---|---|---|---|---|---|---|
| **1** | Fe w/$N_2$ | oleic acid | 1,2-hexadecanediol | octyl ether | Fe $(Acac)_2$ | $N_2$ rather than air |
| **2** | Fe w/ $N_2$ | oleic acid | 1,2-hexadecanediol | octyl ether | Fe $(Acac)_2$ | capping agent concentration reduced by ½ |
| **3** | Fe w/ $N_2$ | oleic acid | 1,2-hexadecanediol | octyl ether | Fe $(Acac)_2$ | capping agent concentration reduced by ¼ |
| **4** | Fe w/ $N_2$ | oleic acid | 1,2-hexadecanediol | octyl ether | Fe $(Acac)_2$ | Repeat of #1,2,and3 |

**Table 3.2** Summary of thermal polyol $Fe^0$ nanoparticle syntheses reagents and conditions

It was believed that removal of oxygen from the reaction vessel could produce a fully reduced iron metal core via the polyol technique. There are published reports of $Co^{+2}$ becoming fully reduced to $Co^0$ via similar polyol techniques at temperatures over 160°C.[51] While the reduction potential of $Co^{+2}$ to $Co^0$ is –0.28 V, and $Fe^{+2}$ to $Fe^0$ has a slightly more negative reduction potential of –0.447 V, it was hypothesized that $Fe^0$ may be produced via similar techniques. The product of this synthesis was a black waxy material whereas powders were produced from the magnetite syntheses. **Figures 3.3** and **3.4** display the FT-IR spectrum and XRD pattern, respectively, of the product from the first $Fe^{+2}$ to $Fe^0$ attempt.

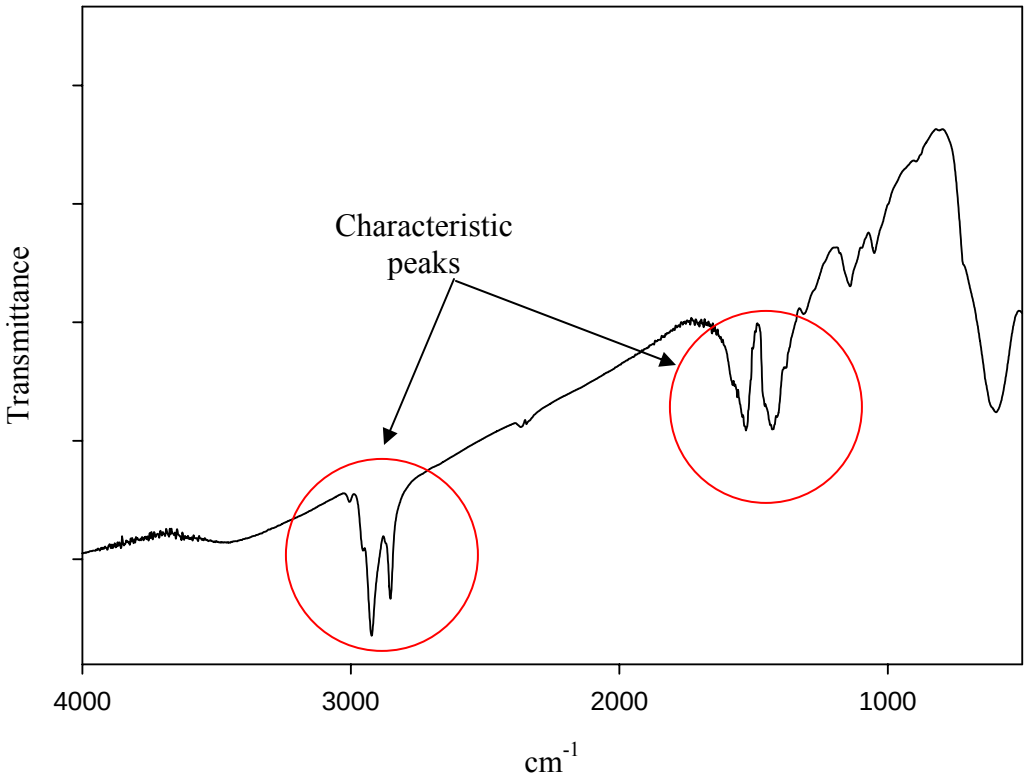


**Figure 3.3** FT-IR spectrum of thermal polyol $Fe^0$ core-shell nanoparticle product

The OH peak is much broader and seems to have shifted to a lower energy in this sample. It has been reported that the *v*(OH) stretching band shifts to higher frequencies when powders are formed.[20] This can be explained by a decrease in hydrogen bonding in the diol medium after formation of the powdered metal.[20] The other characteristic peaks have not changed. The $CO_2$ peak is not present because the instrument was purged with nitrogen. It was not expected that the formation of $Fe^0$ particles would lead to major differences in the FT-IR spectrum as compared to magnetite. FT-IR only verified that the bond between the oleic acid carboxylate group and the metal core was formed, as well as the presence of the carbon chain from the oleic acid capping agent.

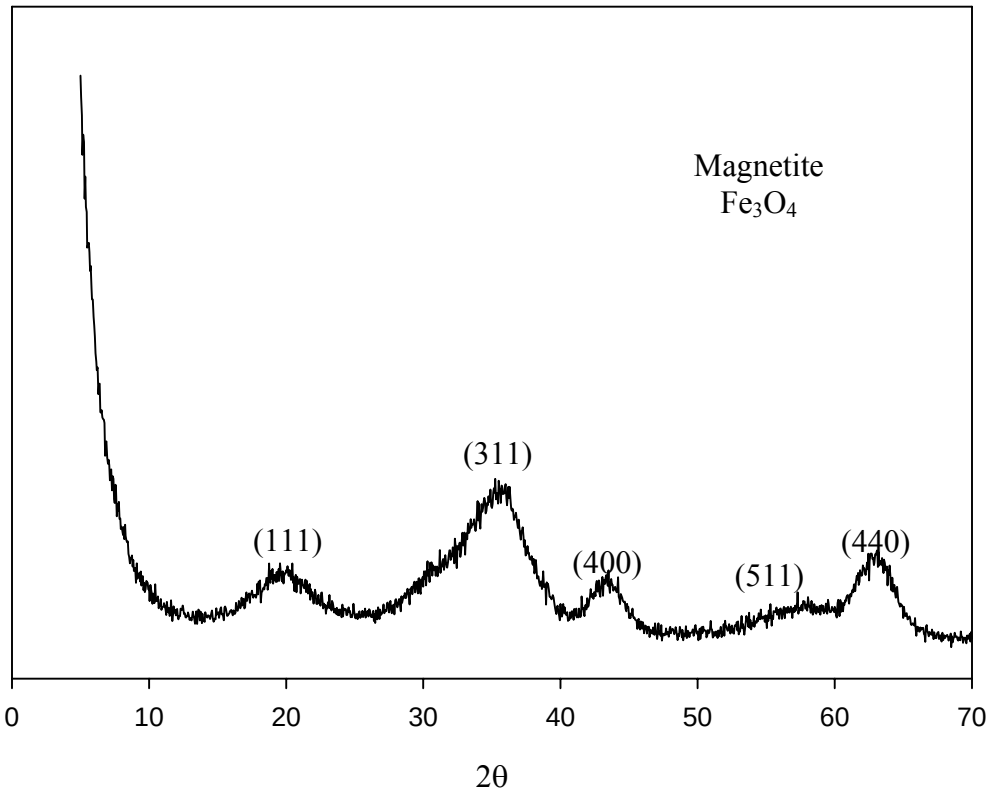


**Figure 3.4** XRD pattern from thermal polyol $Fe^0$ core-shell nanoparticle product with labeled Miller-index planes

Based on comparison to the ICDD database, the XRD pattern indicates some magnetite is present. The peaks are much broader than those from the original magnetite syntheses. Based on the Scherrer equation the particles produced were around 2 nm; much smaller than the particles produced in the previous reactions performed in an ambient environment. Along with smaller sized particles, broad peaks also indicate a more amorphous material might have been produced.[55] The large feature below 10° has been attributed to the silicon sample holder, and is common to most XRD patterns in this work. The presence of a magnetite structure was somewhat surprising as attempts were made to maintain an oxygen free environment. However, the ethanol that was added to

precipitate the nanoparticles was not degassed and may have contained sufficient dissolved oxygen to oxidize the product. Therefore, it cannot be concluded that $Fe^0$ was produced, but it cannot be ruled out either. Evidence of $Fe^0$ in an XRD pattern would consist of one large peak at approximately 45°.[48] This feature is not present in this XRD pattern. Repeat syntheses were performed with similar results.

### 3.3.1 Capping Agent Concentration Investigation of $Fe^0$ Thermal Polyol Method

This investigation was done to determine if the capping agent concentration could affect the ability to produce $Fe^0$ core-shell nanoparticles via the polyol method. **Table 3.3** summarizes the reaction conditions and reagents.

| Sample # | Type | Capping Agent | Reducing Agent | Solvent | Metal Salt | Variation |
|---|---|---|---|---|---|---|
| **1** | Fe w/$N_2$ | oleic acid | 1,2-hexadecanediol | octyl ether | Fe $(Acac)_2$ | $N_2$ rather than air |
| **2** | Fe w/ $N_2$ | oleic acid | 1,2-hexadecanediol | octyl ether | Fe $(Acac)_2$ | capping agent concentration reduced by ½ |
| **3** | Fe w/ $N_2$ | oleic acid | 1,2-hexadecanediol | octyl ether | Fe $(Acac)_2$ | capping agent concentration reduced by ¼ |

**Table 3.3** Summary of thermal polyol capping agent concentration investigation reagents and conditions

The FT-IR spectra of the three different capping agent concentrations (1 mmol, 0.5 mmol, and 0.75 mmol) are shown in **Figure 3.5.** Comparing the three FT-IR spectra, the ratios of the $\nu_s$(C=O) and $\nu_a$(C=O) stretching modes to the $\nu_s$(-$CH_2$) and $\nu_a$(-$CH_2$) stretching appeared to decrease as the capping agent concentration was reduced with the

most dramatic change being observed when the concentration was reduced to one half of the original. All three appear to be capped by the oleic acid.

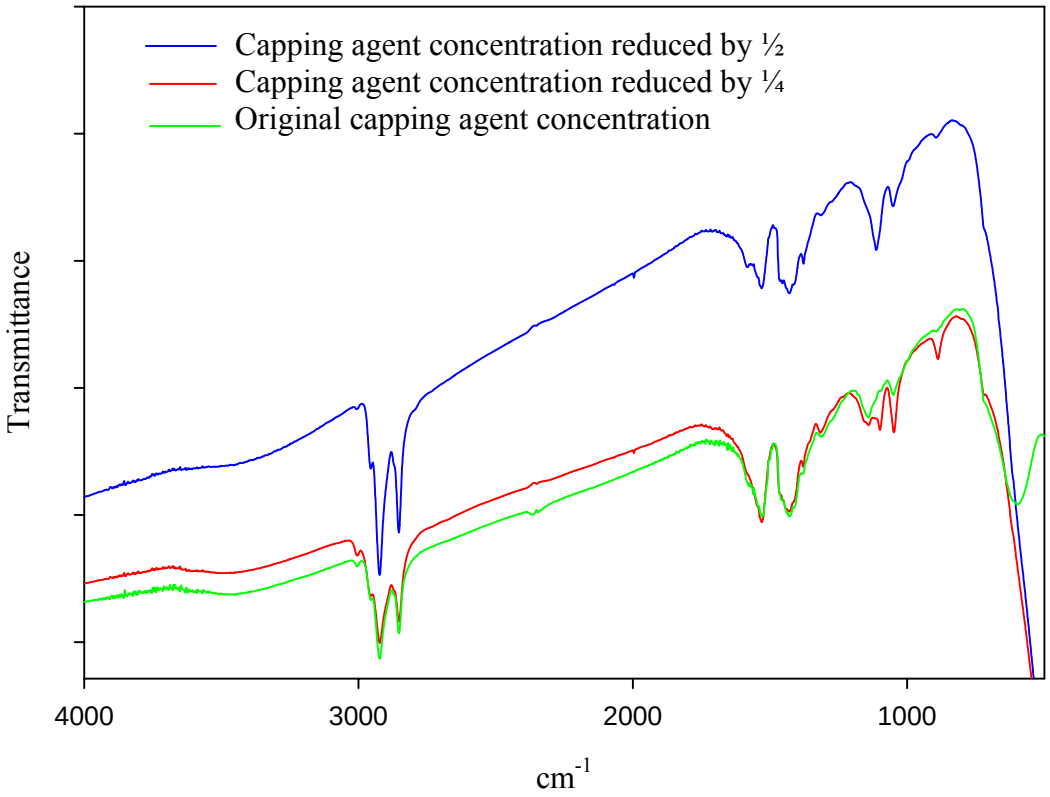


**Figure 3.5** FT-IR spectra comparison of different capping agent concentration products prepared by thermal polyol $Fe^0$ core-shell nanoparticle synthesis

All three XRD patterns (**Figure 3.6**) have been identified as magnetite. All peaks are very broad indicating that fairly small and/or amorphous particles were produced. When the oleic acid concentration was significantly reduced (50% reduction), more pronounced and broader features were noted in the lower angles. The ratio between the features at approximately 20° and that at approximately 35° is seemingly inverted as the capping agent concentration is decreased. Large low angle features like this could be

related to interlayer spacing in lamellar structures.[51] This is the opposite of what one would expect, because if less capping agent is present (less organic material) the feature indicating organic material should decrease rather than increase. This observation has not been successfully explained.

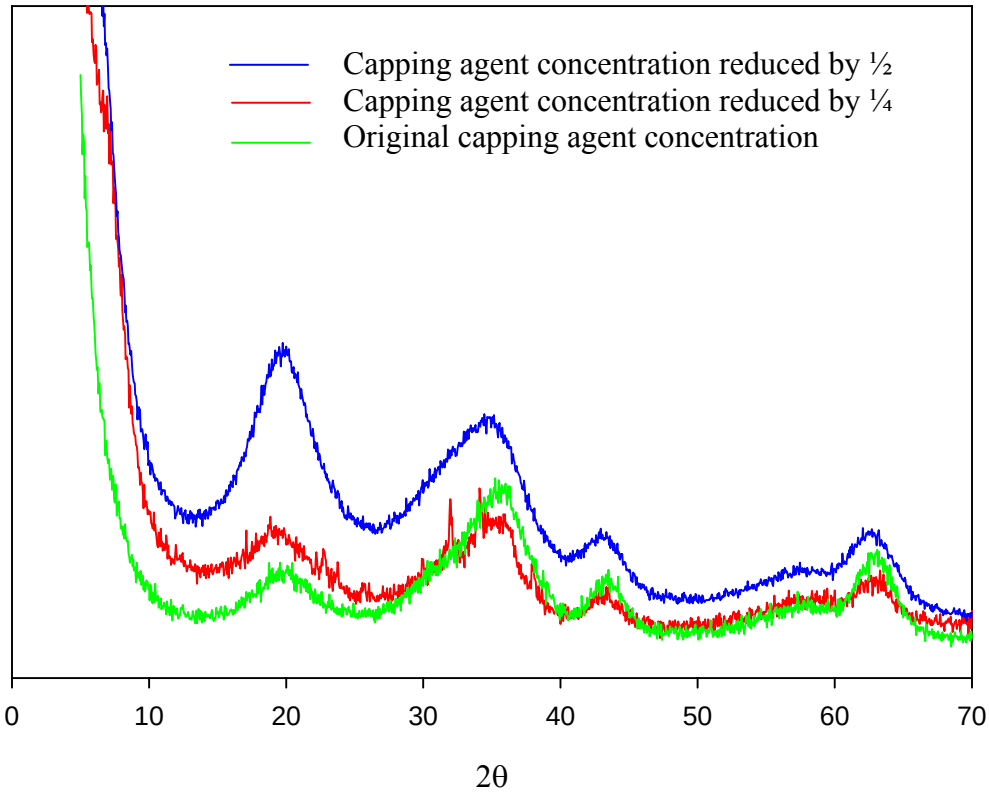


**Figure 3.6** XRD pattern from three different capping agent concentration products prepared by thermal polyol $Fe^0$ core-shell nanoparticle synthesis

### 3.3.2 Iron Oxidation State Investigation via Thermal Polyol Method

For this synthesis attempt, the iron salt was changed from an iron (II) source to iron (III) bromide. It was unclear whether the previous attempts had been successful in producing $Fe^0$ core-shell nanoparticles simply by the removal of oxygen. As mentioned previously, $Co^{+2}$ to $Co^0$ has been successfully achieved via the polyol method[14,51] and has an associated reduction potential of –0.28 V. Therefore, it was hypothesized that $Fe^0$ could be produced from an Fe (III) salt. $Fe^{+3}$ to $Fe^0$ has a reduction potential of –0.037 V. This means it should be easier to reduce than $Co^{+2}$, but ligands play a big role in the actual reduction potential of metals. Reagents and conditions for this reaction are summarized in **Table 3.4**

| Sample # | Type | Capping Agent | Reducing Agent | Solvent | Metal Salt |
|---|---|---|---|---|---|
| **1** | $FeBr_3$ w/ $N_2$ | oleic acid | 1,2-hexadecanediol | octyl ether | $FeBr_3$ |
| **2** | $FeBr_3$ w/ $N_2$ | oleic acid | 1,2-hexadecanediol | octyl ether | $FeBr_3$ |

**Table 3.4** Summary of thermal polyol $Fe^0$ nanoparticle syntheses reagents and conditions

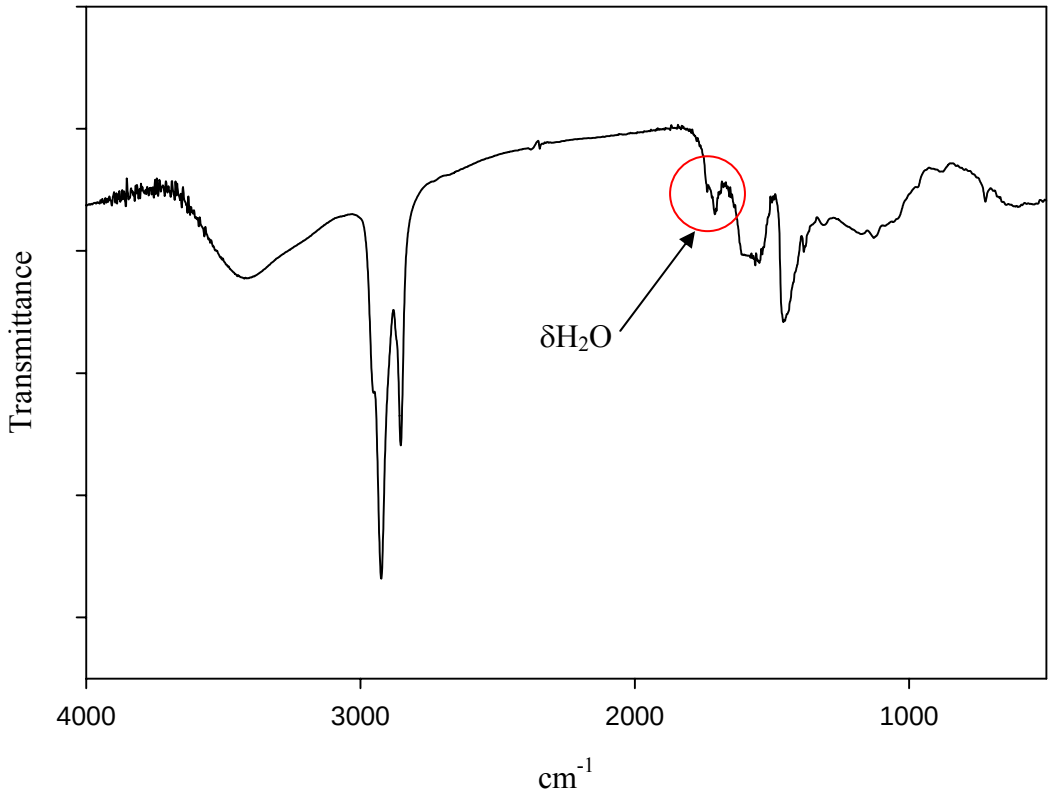


**Figure 3.7** FT-IR spectrum of the thermal polyol $Fe^0$ core-shell nanoparticle product prepared with $FeBr_3$

A black waxy product was produced from this reaction. The FT-IR spectrum of the sample (**Figure 3.7**) indicates the bond has been formed with the oleic acid and the metallic core. The IR bands in the 2850-2960 $cm^{-1}$ region arise from the $\nu_s(\text{-}CH_2)$ and $\nu_a(\text{-}CH_2)$ stretching of the oleic acid carbon chain.[12,29,52] A broad $\nu$(OH) stretch at 3400 $cm^{-1}$ is present as well. The two signature bands at 1600 $cm^{-1}$ and 1480 $cm^{-1}$ that correspond to $\nu_s$(C=O) and $\nu_a$(C=O) indicating a bond has formed between the particle and the capping agent are present as well. All other bands below 2000 $cm^{-1}$ are due to the $\nu$(C-C) stretch, $\nu$(C-O) stretches, $CH_2$ deformations and other motions that are too

complex to assign[51,52] and indicate the oleic acid chain is still present. The sharp band at 1620 $cm^{-1}$ has been attributed to a $\delta H_2O$ vibration ($\delta$ signifies an in phase rock).[51]

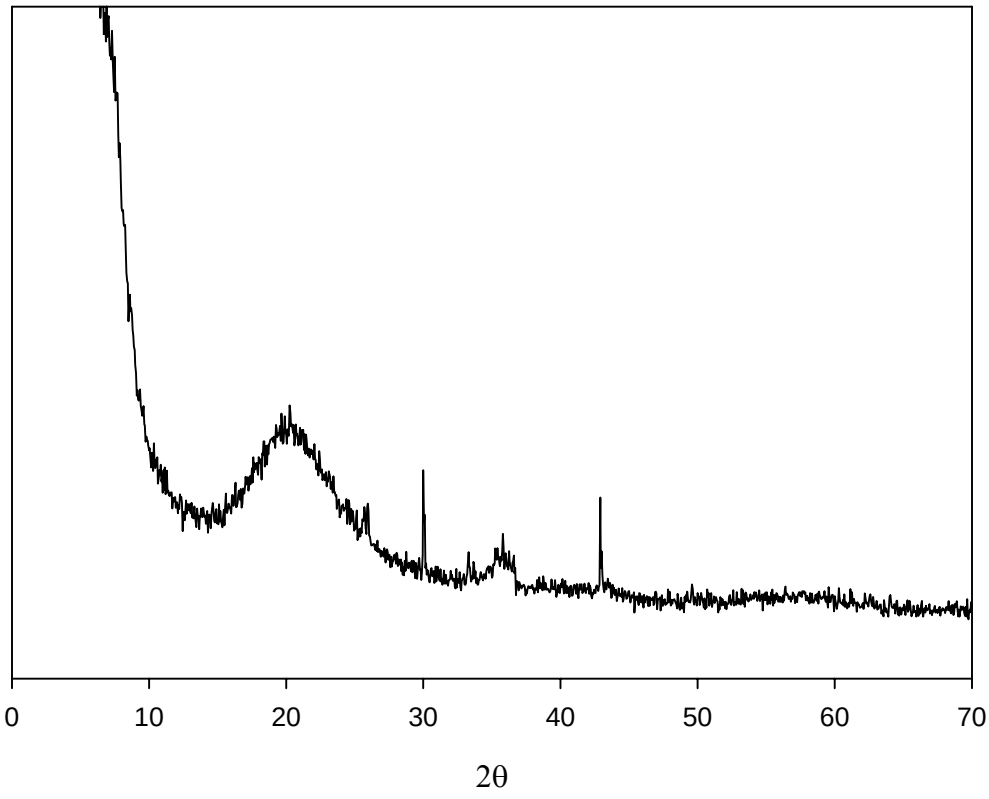


**Figure 3.8** XRD pattern from thermal polyol $Fe^0$ core-shell nanoparticle product prepared with $FeBr_3$

The XRD pattern from the product (**Figure 3.8**) is significantly different than any previous XRD patterns. There is no clear magnetite structure. However, there is no clear feature present at approximately 45° either. The large feature at approximately 20° may arise from an amorphous iron core or possibly the oleic acid capping agent. There are a few very sharp features that have been attributed to noise because all other features are broad in nature.

### 3.3.3 Microwave Synthesis Attempt of $Fe^0$ Core-shell Nanoparticles

Based on published reports, higher temperatures seem to facilitate the reduction of metal salts via the polyol technique.[15,51] Microwave energy was investigated for possible higher reaction temperatures in localized hot spots analogous to those seen in sonochemical reactions. Sonochemical methods have been successful in producing amorphous $Fe^0$ core-shell nanoparticles.[46] The sonochemical method of producing these $Fe^0$ particles relies on localized hot spots created by acoustic cavitations in the hydrocarbon solvent. Therefore, the microwave polyol technique was applied in attempts to produce $Fe^0$ core-shell nanoparticles. A summary of reagents used in the microwave syntheses are listed in **Table 3.5**.

| Sample # | Type | Capping agent | Reducing agent | Solvent | Metal Salt | Variation |
|---|---|---|---|---|---|---|
| **MW1** | Fe | oleic acid | 1,2-hexadecanediol | octyl ether | $Fe(Acac)_2$ | microwave heat source (30min) |
| **MW2** | Fe | oleic acid | 1,2-hexadecanediol | octyl ether | $Fe(Acac)_2$ | Repeat of MW1 |
| **MW3** | Fe | oleic acid | 1,2-hexadecanediol | octyl ether | $Fe(Acac)_2$ | Repeat of MW1 |
| **MW4** | Fe | oleic acid | 1,2-hexadecanediol | octyl ether | $Fe(Acac)_2$ | Repeat of MW1 |
| **MW5** | Fe | oleic acid | 1,2-hexadecanediol | octyl ether | $Fe(Acac)_2$ | Repeat of MW2 |

**Table 3.5** Summary of microwave polyol $Fe^0$ nanoparticle syntheses reagents and conditions

Unfortunately, the octyl ether has a very low dielectric constant, and does not absorb microwave energy efficiently enough to achieve the temperatures reached during thermal heating. Thermal heating brought the temperature of the solution to its boiling point; 270°C, while microwave heating only achieved 190°C.

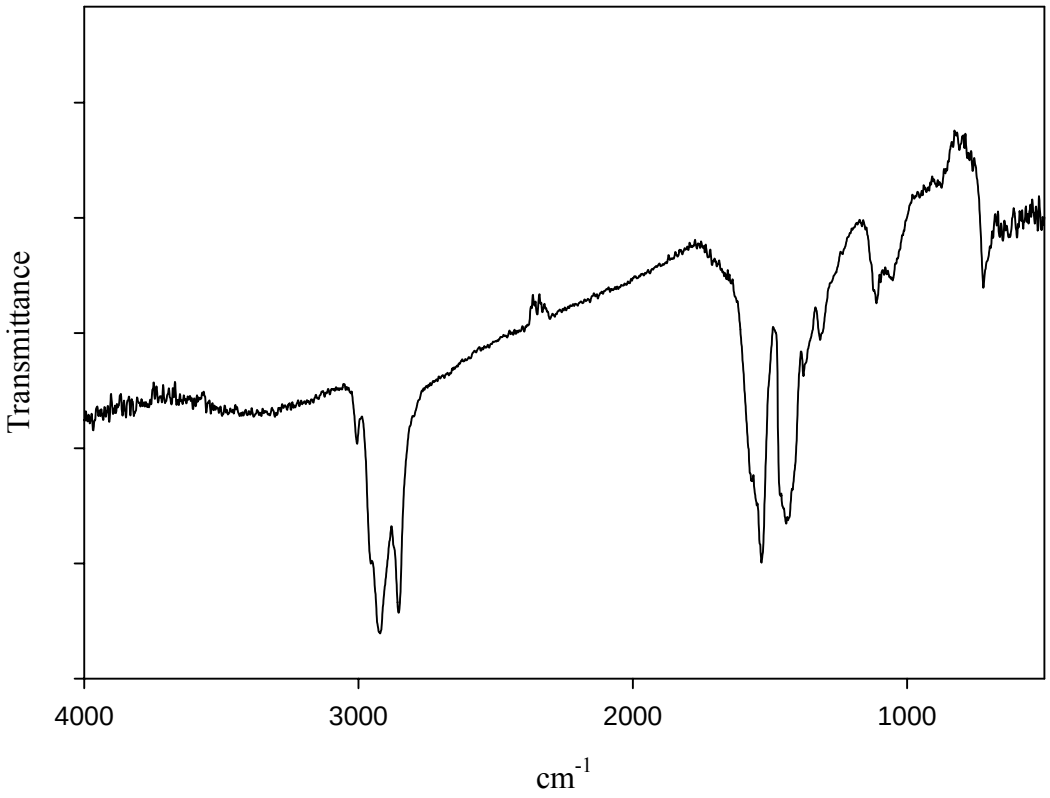


**Figure 3.9** FT-IR spectrum of the microwave polyol $Fe^0$ core-shell nanoparticle product

The product of this reaction was a black waxy solid. The FT-IR spectrum from the microwave polyol $Fe^0$ core-shell nanoparticle synthesis (**Figure 3.9**) indicates that the oleic acid has bonded to the metal surface. The ratio of the $\nu_s$(C=O) and $\nu_a$(C=O) bands to the $\nu_s$(-$CH_2$) and $\nu_a$(-$CH_2$) bands is much higher in this spectrum than in previous spectra. This could indicate that a larger concentration of oleic acid is bonded to the surface of the particles. The $\nu$(OH) stretch is very broad and shifted to lower energies, similar to the thermal polyol $Fe^0$ particle attempt (**Figure 3.3**).

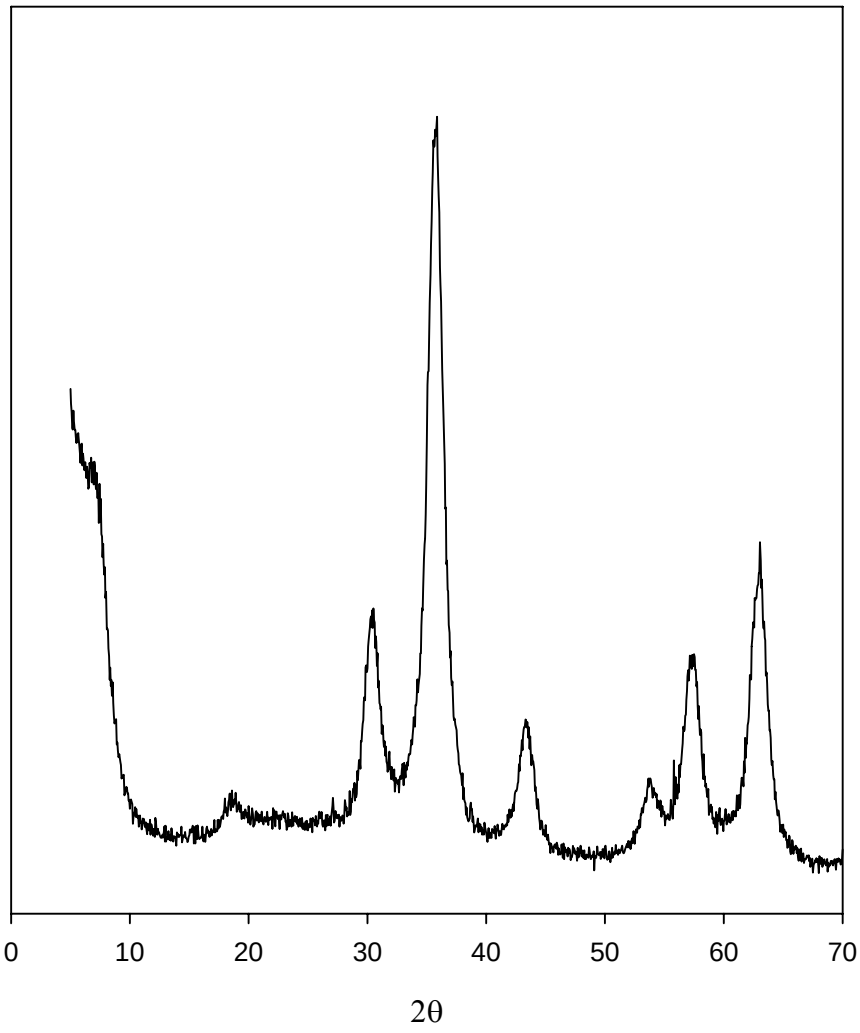


**Figure 3.10** XRD pattern of microwave polyol $Fe^0$ core-shell nanoparticle product

As is evident from the XRD pattern of this product (**Figure 3.10**), magnetite was again formed. However, the peaks in the XRD are a lot sharper than the thermal $Fe^0$ core-shell nanoparticle synthesis attempt (**Figure 3.4**); more similar to the produces from the thermal magnetite syntheses (**Figure 3.2**). Again, these sharp peaks indicate the presence of a more crystalline structure. Also, larger particles were possibly produced.

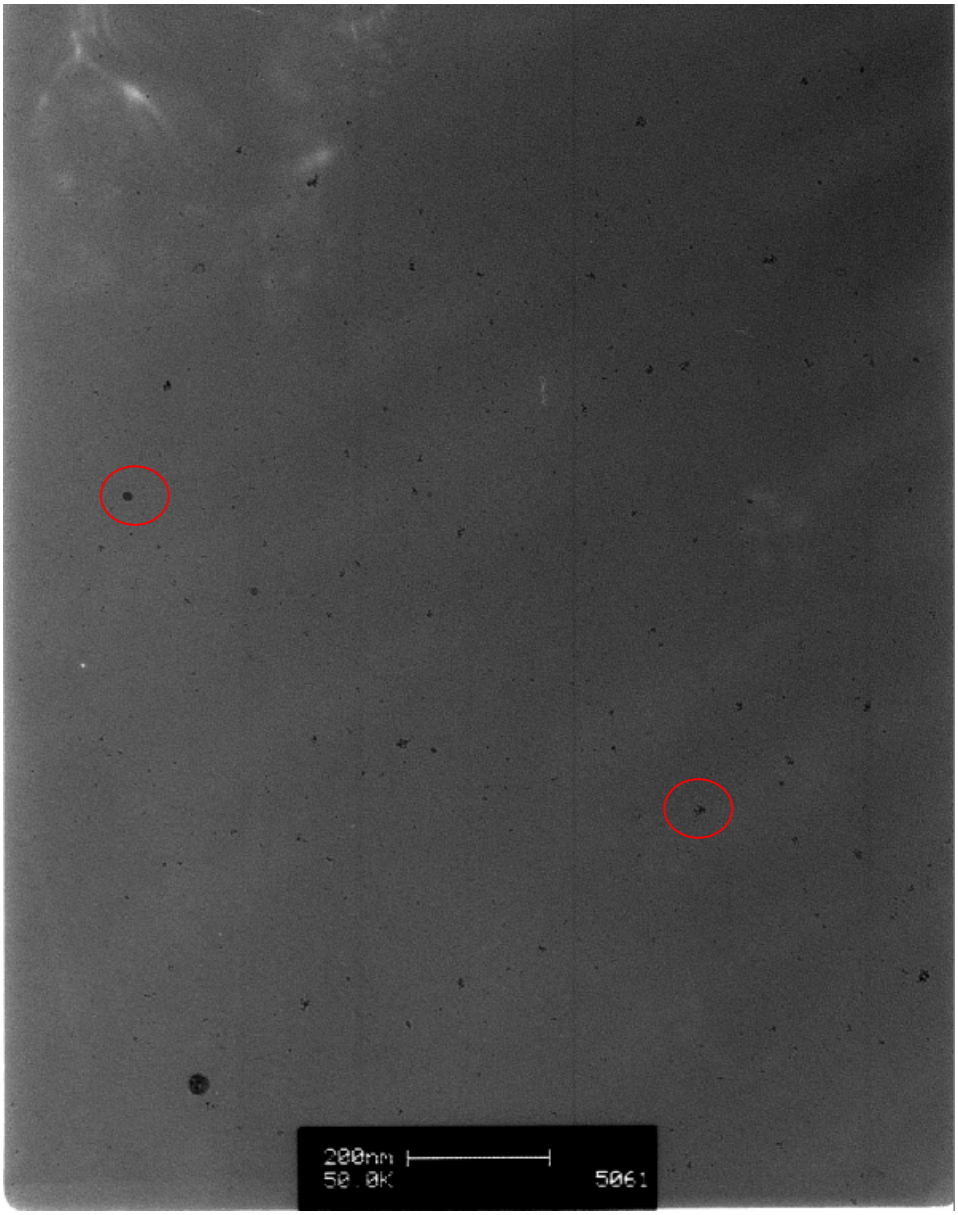


**Figure 3.11** TEM image of particles produced from microwave polyol $Fe^0$ core-shell nanoparticle synthesis

TEM was employed to verify that spherical nanoparticles were produced from this synthesis. The TEM image **(Figure 3.11)** indicates that fairly mono-dispersed spherical particles were produced. The particles are in the 3-15 nm size range, which are larger than the thermal $Fe^0$ estimated particle size, which could explain why the peaks in the XRD pattern are sharper than the thermal $Fe^0$ product XRD pattern. After this initial

synthesis attempt failed to definitively produce $Fe^0$, repeat syntheses were performed, but similar results were obtained.

### 3.3.4 Solvent/Reducing Agent Investigation (1,2-hexanediol)

Microwave energy was investigated because the localized hot spots produced during microwave syntheses could possibly facilitate the creation of an amorphous $Fe^0$ core-shell nanoparticle. However, the dioctyl ether solvent has a very low dielectric constant, and therefore did not couple well with the microwaves. The bulk solution did not reach the temperatures that were reached in thermal heating (190°C vs. 270°C). Because the solvent was not being heated, this meant the solvated iron salt was absorbing the microwave energy. It has been reported that localized superheated regions, induced from the interactions of microwave radiation with a metal powder, can enhance the yield of a specific reaction without a significant change in the average temperature.[56] Unfortunately, the desired results were not achieved with this set of reaction conditions.

Therefore, it was postulated that changing to a more polar solvent could produce different results. Most polyol reactions from the literature use the polyol as the solvent and the reducing agent. The most commonly used polyols are ethylene glycol and tetraethylene glycol. Up to this point a solid diol reducing agent was used and dissolved in an ether solvent. For the next set of experiments 1,2-hexanediol was chosen as the new solvent/reducing agent because it has a much higher dielectric constant and should be able to reach temperatures similar to those observed with thermal heating. Capping agent and iron salt were also changed during the course of these experiments, but there was no observed difference in the product's characteristics based on these variations. To the best of our knowledge there are no published reports utilizing this solvent/reducing

agent in the polyol method. **Table 3.6** summarizes the reaction conditions and reagents for these syntheses.

| Sample # | Type | Capping Agent | Reducing Agent | Solvent | Metal Salt | Variation |
|---|---|---|---|---|---|---|
| **MW1** | Fe | oleic acid | 1,2-hexanediol | 1,2-hexanediol | Fe $(Acac)_2$ | changed red agent/solvent |
| **MW2** | Fe | oleic acid | 1,2-hexanediol | 1,2-hexanediol | Fe $(Acac)_2$ | reduced by 1/2 |
| **MW3** | Fe | oleic acid | 1,2-hexanediol | 1,2-hexanediol | Fe $(Acac)_2$ | scaled up by 2 from MW10 |
| **MW4** | Fe | oleic acid | 1,2-hexanediol | 1,2-hexanediol | Fe (II) acetate | changed iron source |
| **MW5** | Fe | oleic acid | 1,2-hexanediol | 1,2-hexanediol | Fe (II) acetate | Repeat of MW20 |
| **MW6** | Fe | PVP | 1,2-hexanediol | 1,2-hexanediol | Fe (II) acetate | changed capping agent |
| **MW7** | Fe | PVP | 1,2-hexanediol | 1,2-hexanediol | Fe (II) acetate | Repeat of MW22 |

**Table 3.6** Summary of microwave polyol $Fe^0$ nanoparticle syntheses reagents and conditions

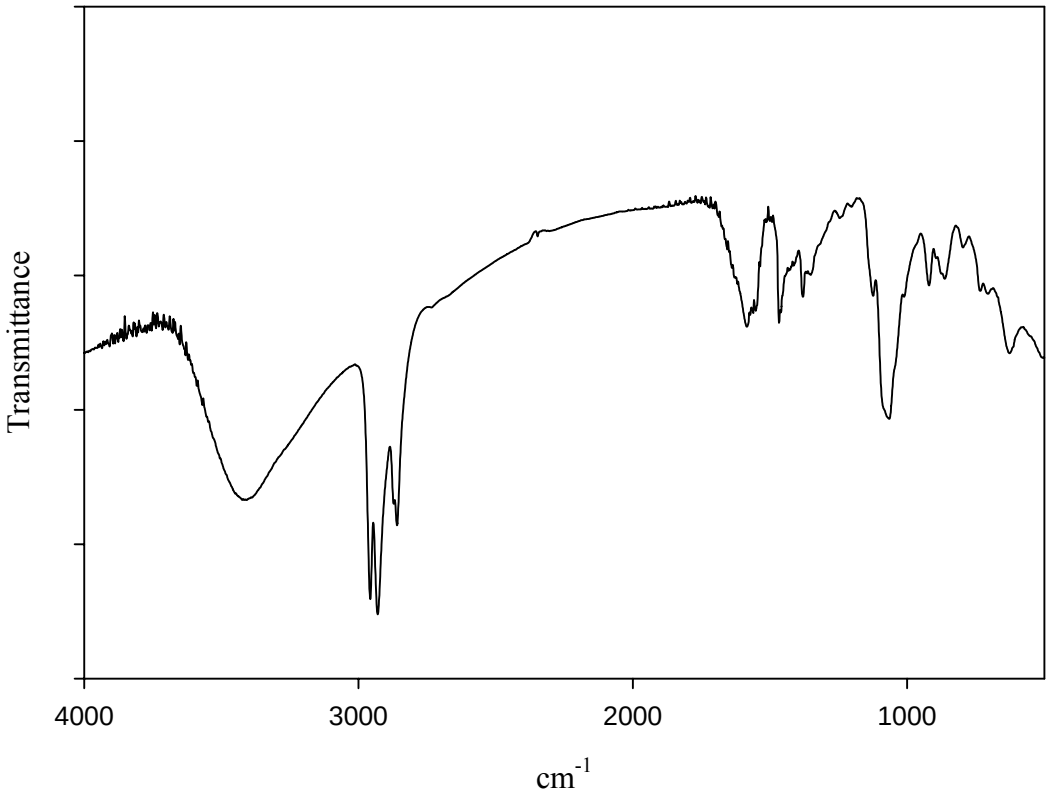


**Figure 3.12** FT-IR spectrum of the microwave polyol $Fe^0$ core-shell nanoparticle synthesis product prepared with 1,2-hexanediol

The product of this synthesis was a tan powder. The FT-IR spectrum of the product prepared with 1,2-hexanediol (**Figure 3.12**) resembled the FT-IR spectra from the samples that were sparged with air during thermal heating (**Figure 3.1**). The *ν*(OH) stretch at 3400 $cm^{-1}$ is very prevalent, and similar to the *ν*(OH) stretch in the other spectra of powders rather than waxes. There are a few features around 1000$cm^{-1}$ that have been attributed to *ν*(C-O) stretches. These features along with the very pronounced OH peak are possibly due to residual diol in the sample. The other characteristic peaks such as the $\nu_s(\text{-}CH_2)$ and $\nu_a(\text{-}CH_2)$ peaks in the 2850-2960 $cm^{-1}$ region, and the two signature bands at

1600 $cm^{-1}$ and 1480 $cm^{-1}$ that correspond to the $\nu_s$(C=O) and $\nu_a$(C=O) stretching modes respectively,[29] of the oleic acid carbon chain are present as well.

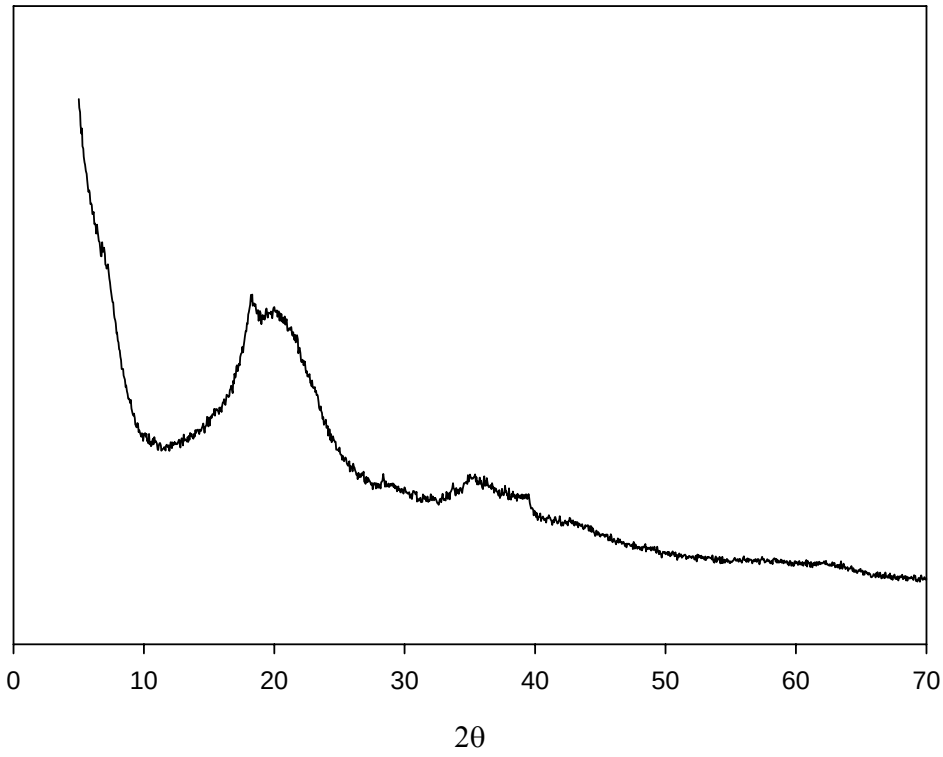


**Figure 3.13** XRD pattern from microwave polyol $Fe^0$ core-shell nanoparticle synthesis product prepared with 1,2-hexane diol

This XRD pattern (**Figure 3.13**) resembles that of $Fe^0$ core-shell nanoparticle synthesis attempts using $FeBr_3$ (**Figure 3.8**). The large feature at approximately 20° indicates the presence of an amorphous material, possibly a large amount of organic material. Similar features have been reported when producing Co oxide nanoparticles in different isomers of butane diol.[51] According to these reports, the presence of a strong low-angle reflection is related to interlayer spacing in lamellar structures. This is an indication that stacked metal-oxygen sheets separated by bonded alkoxide ions are

present.[51] This feature could also be attributed to residual diol in the sample which is further supported by the FT-IR data. Even though there was no clear structure based on the XRD pattern, TEM (**Figure 3.14**) indicates nanoparticles were produced.

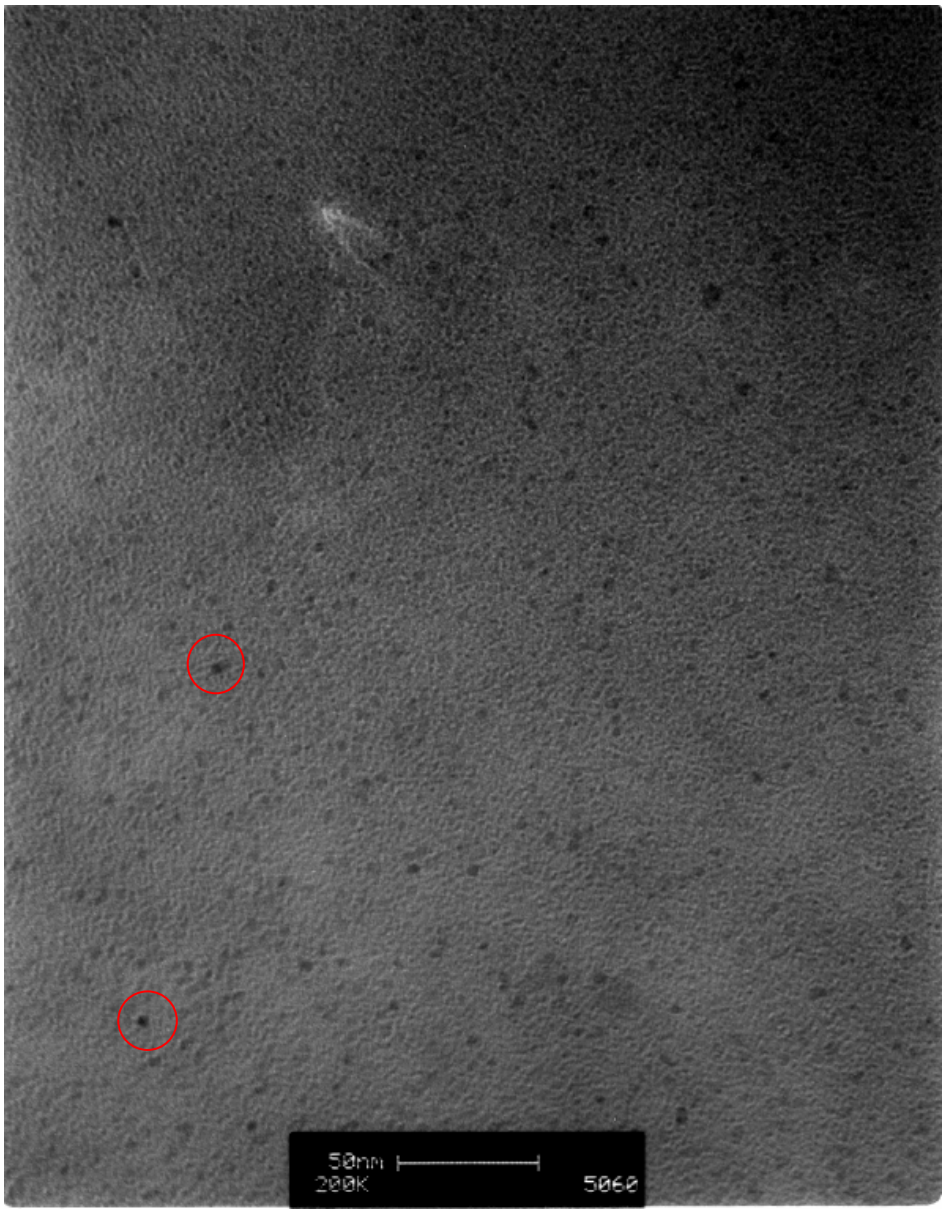


**Figure 3.14** TEM image of particles produced from microwave polyol $Fe^0$ synthesis prepared with 1,2-hexanediol

The TEM image of the particles from this synthesis indicates that a fairly wide range of sizes were produced. The particles appear to be spherical and range from

4 to 20 nm in diameter. After these new results were attained, additional syntheses were performed and similar results were achieved.

### 3.3.5 Solvent/Reducing Agent Investigation (Polyethylene Glycol MW 600 g/mol)

In this set of experiments, PEG MW 600 g/mol was investigated as a possible reducing agent/solvent for the microwave polyol method of synthesizing $Fe^0$ core-shell nanoparticles from an iron salt. **Table 3.7** summarizes the reaction conditions and reagents used in these syntheses.

| Sample # | Type | Capping Agent | Reducing Agent | Solvent | Metal Salt |
|---|---|---|---|---|---|
| **MW1** | Fe | oleic acid | PEG | PEG | $Fe(Acac)_2$ |
| **MW2** | Fe | oleic acid | PEG | PEG | $Fe(Acac)_2$ |

**Table 3.7** Summary of microwave polyol $Fe^0$ nanoparticle syntheses reagents and conditions

To our knowledge, there have not been any published reports of this particular PEG being used as a solvent/reducing agent for this method. The FT-IR spectrum of the product (**Figure 3.15**) did show the two characteristic $\nu_s$(C=O) and $\nu_a$(C=O) stretching modes indicating that the particles had been capped with the oleic acid. The $\nu$(C=O) stretch at 1710 $cm^{-1}$ is absent from the spectrum, which also indicates the particles were capped with the oleic acid. There are numerous features around 1000$cm^{-1}$ that have been attributed to the $\nu$(C-C) stretch, $\nu$(C-O) stretches, $CH_2$ deformations and other motions that are too complex to assign[51,52]. These features along with the very pronounced $\nu$(OH) peak are possibly due to residual diol in the sample.

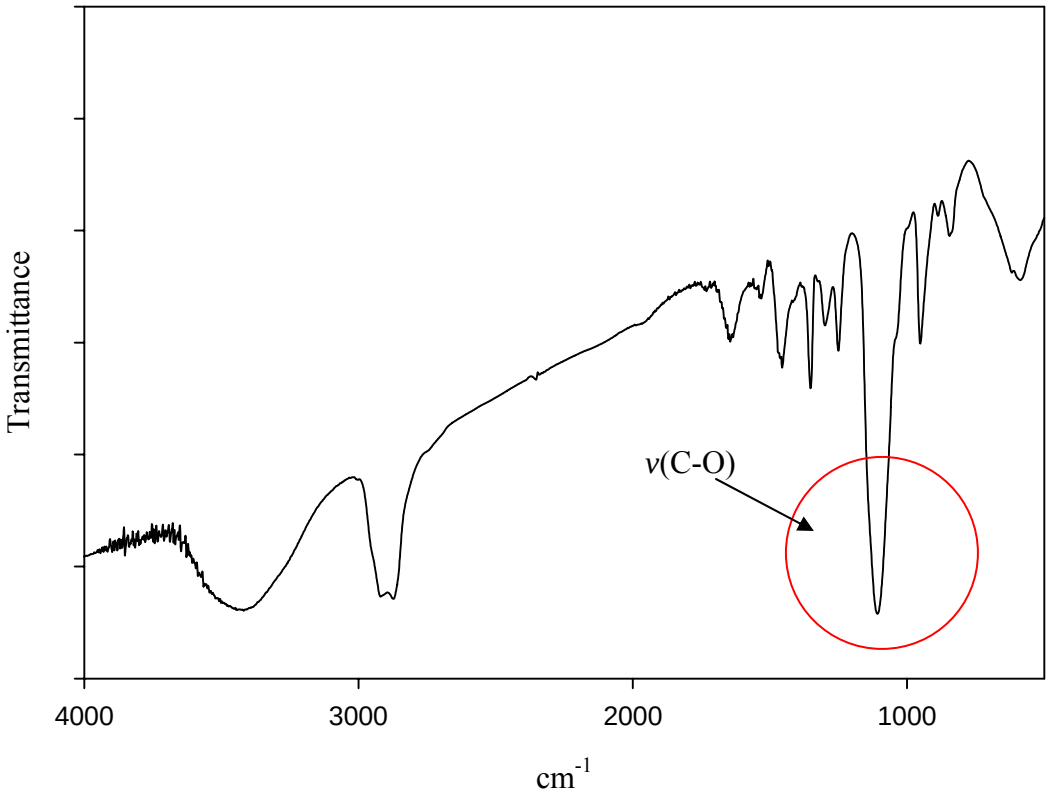


**Figure 3.15** FT-IR spectrum of microwave polyol $Fe^0$ core-shell nanoparticle synthesis product prepared with PEG

The XRD pattern of the product from this synthesis (**Figure 3.16)** looked similar to those from the 1,2-hexanediol syntheses (**Figure 3.13)**. There appears to be an underlying magnetite structure in the XRD pattern. The large feature at approximately 20° is present as it was in the 1,2-hexanediol syntheses, but the (311) peak at approximately 36° from magnetite is also apparent. It can not be concluded that $Fe^0$ or magnetite particles were produced from this synthesis. Repeat syntheses were performed with similar results being observed.

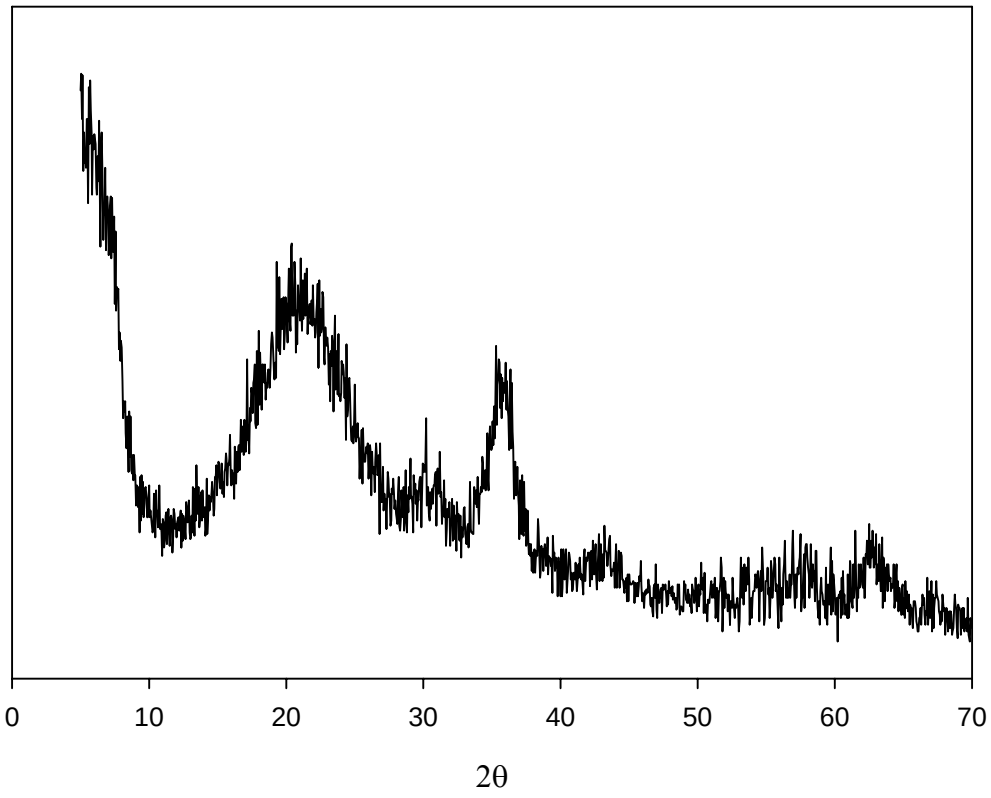


**Figure 3.16** XRD pattern of microwave polyol $Fe^0$ core-shell nanoparticle product prepared with PEG

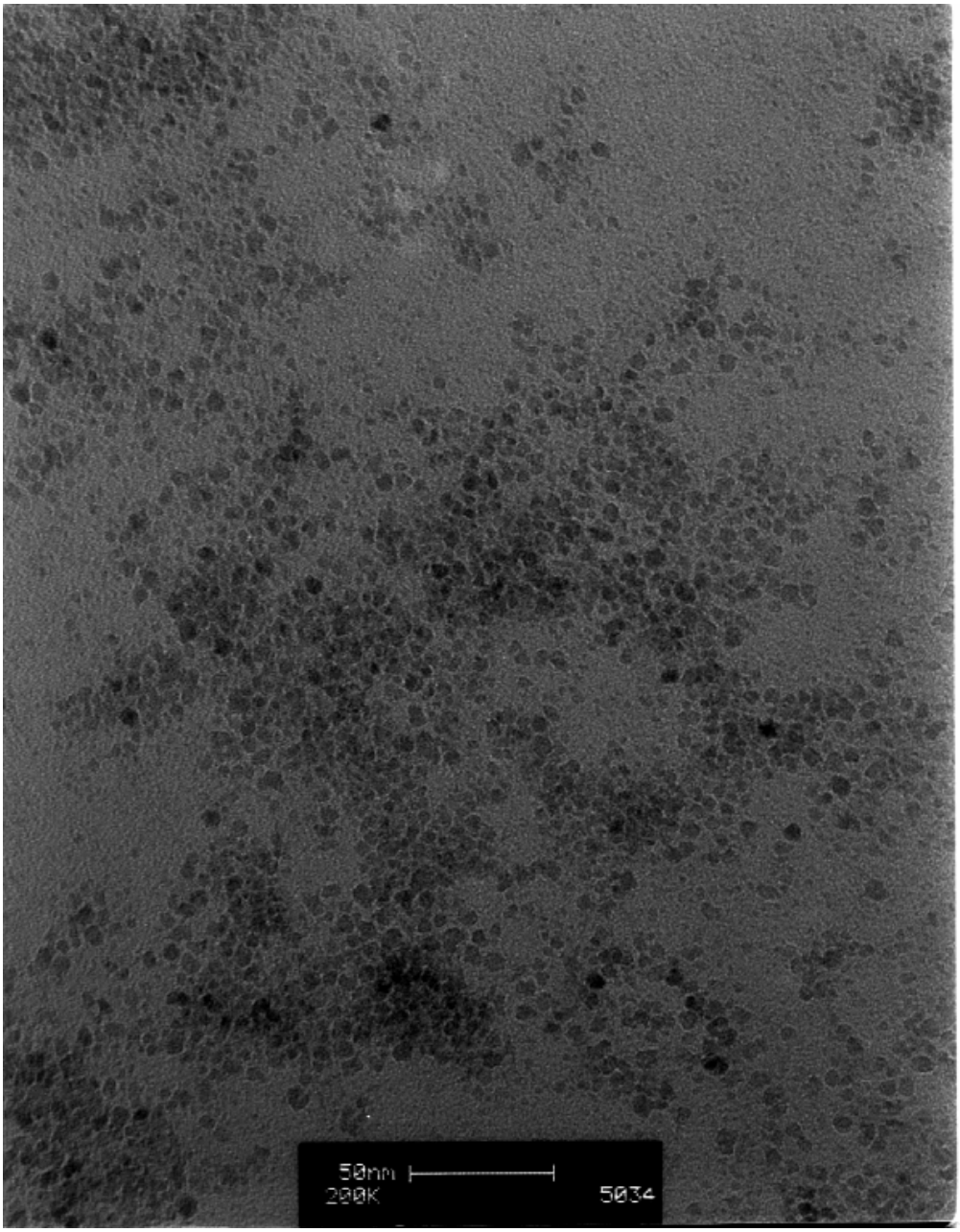


**Figure 3.17** TEM image of particles produced from microwave polyol $Fe^0$ iron core-shell nanoparticle synthesis prepared with PEG

Based on the TEM image (**Figure 3.17**) of the nanoparticles formed during this reaction, it appears that the particles are larger than the previous samples (10-20 nm). It also appears that there is much more agglomeration of the particles. It has been reported that particles produced in ethylene glycol possibly contain the diol along with capping

agent in their organic shell.[20] There are also reports of higher molecular weight PEG (MW 3000 g/mol) used as a capping agent for particles produced via microwave polyol.[11]

### 3.3.6 Microwave Magnetite Synthesis With 1,2-hexanediol and Oleylamine Co-capping Agent

Up to this point, it was concluded that magnetite core-shell nanoparticles had been produced from thermal and microwave heating for the polyol method. These nanoparticles were produced by following a published procedure that involved 1,2-hexadecanediol dissolved in a long chain ether as the solvent/reducing agent. During the course of the investigation into the polyol technique, 1,2-hexanediol proved to be an interesting solvent/reducing agent. A disadvantage to 1,2-hexanediol vs. the ether was the difficulty in removing the high boiling point diol from the precipitate. A benefit was the elimination of the precipitation step with ethanol.

It was unclear if 1,2-hexanediol had succeeded in producing $Fe^0$ particles, because techniques such as X-ray photoelectron spectroscopic (XPS) technique, which has been used in the literature to characterize amorphous iron nanoparticles[8], was not available. However, it was clear that magnetite core-shell nanoparticles had not been produced with 1,2-hexanediol. In order to try to reproduce the magnetite core-shell nanoparticles, the co-capping agent oleylamine was used as per the original magnetite procedure.[33,49] It has been reported that the use of oleic acid and oleylamine together yields a greater amount of magnetite particles than either one alone.[57] The bonding of oleylamine to the magnetite particle has been explained by its coordination to Fe (III) on the surface of the magnetite particle. [57] **Table 3.8** summarizes the reagents and reaction conditions.

| Sample # | Type | Capping Agent | Reducing Agent | Solvent | Metal Salt | Variation |
|---|---|---|---|---|---|---|
| **MW1** | Fe | oleic acid/oleylamine | 1,2-hexanediol | 1,2-hexanediol | Fe (II) acetate | change solvent/red agent and Fe salt |
| **MW2** | Fe | oleic acid/oleylamine | 1,2-hexanediol | 1,2-hexanediol | Fe (II) acetate | change solvent/red agent and Fe salt |

**Table 3.8** Summary of microwave polyol magnetite syntheses reagents and conditions

A black waxy material was produced from this reaction. The FT-IR spectrum of the product (**Figure 3.18**) indicates that the particles formed from this reaction were capped by both capping agents. Not only is the $\nu$(C=O) mode at 1710 $cm^{-1}$ from the COOH group absent, but the $\nu$(N-H) of the $NH_2$ at 3300 $cm^{-1}$ is also absent. This indicates both the capping agents are bonded to the nanoparticle surface. The ratio of the $\nu_s$(C=O) and $\nu_a$(C=O) peaks to the $\nu_s$(-$CH_2$) and $\nu_a$(-$CH_2$) peaks is increased significantly in this spectrum. This could be due to more capping agent bonding to the surface of the metal nanoparticle.

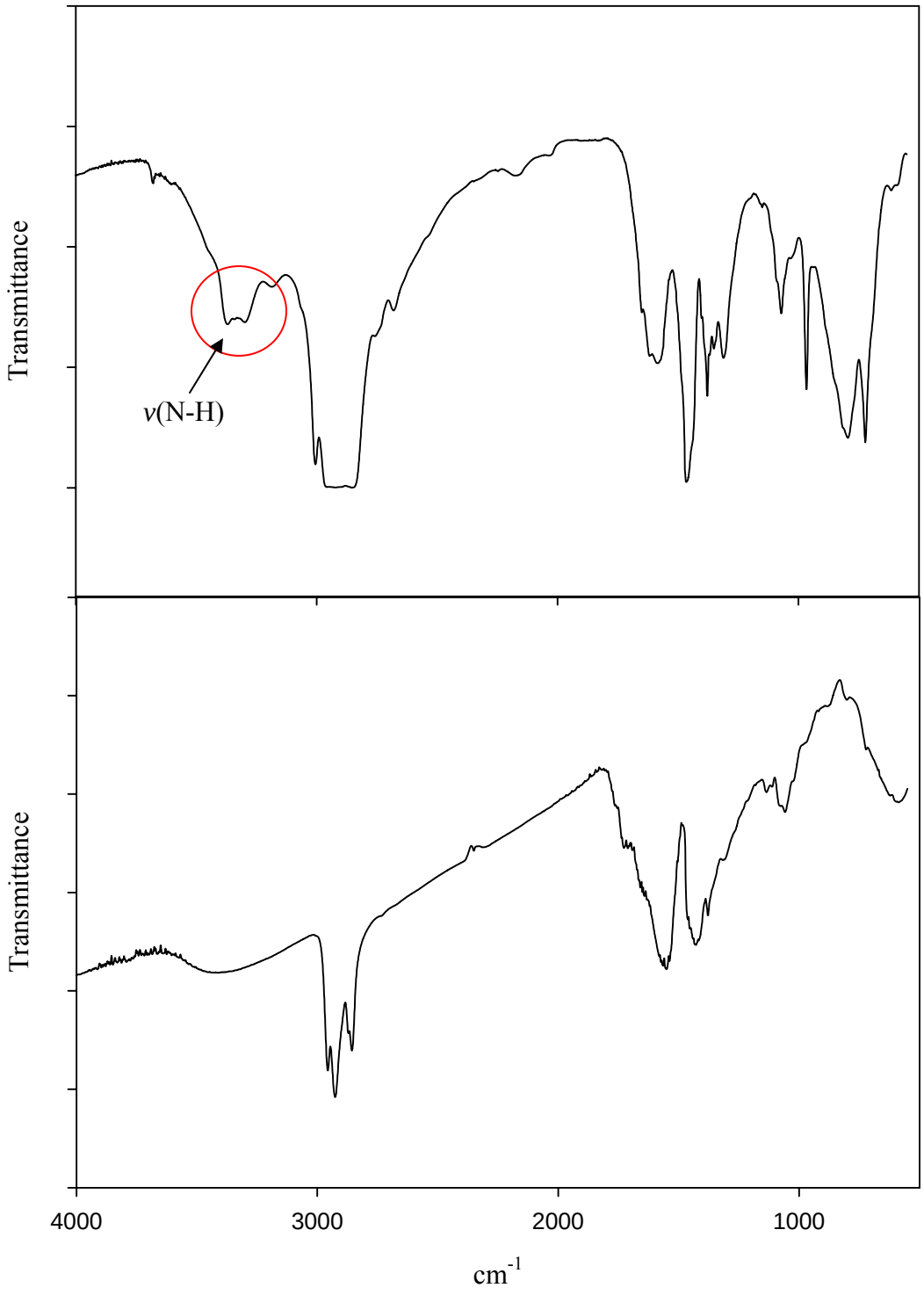


**Figure 3.18** (top) FT-IR spectrum of oleylamine and (bottom) FT-IR spectrum from microwave polyol core-shell magnetite nanoparticle synthesis product prepared with 1,2-hexanediol and oleylamine co-capping agent

The XRD pattern (**Figure 3.19**) indicates a magnetite structure. There is a difference in the magnetite XRD pattern produced from this reaction vs. the magnetite XRD patterns produced previously (**Figure 3.2** and **Figure 3.10**). There is a large broad feature at approximately 20°. This feature could be attributed to a large amount of organic molecules present or a lamellar structure. This was the first time this solvent was successfully removed, and the first instance of microwave heating producing magnetite with 1,2-hexanediol.

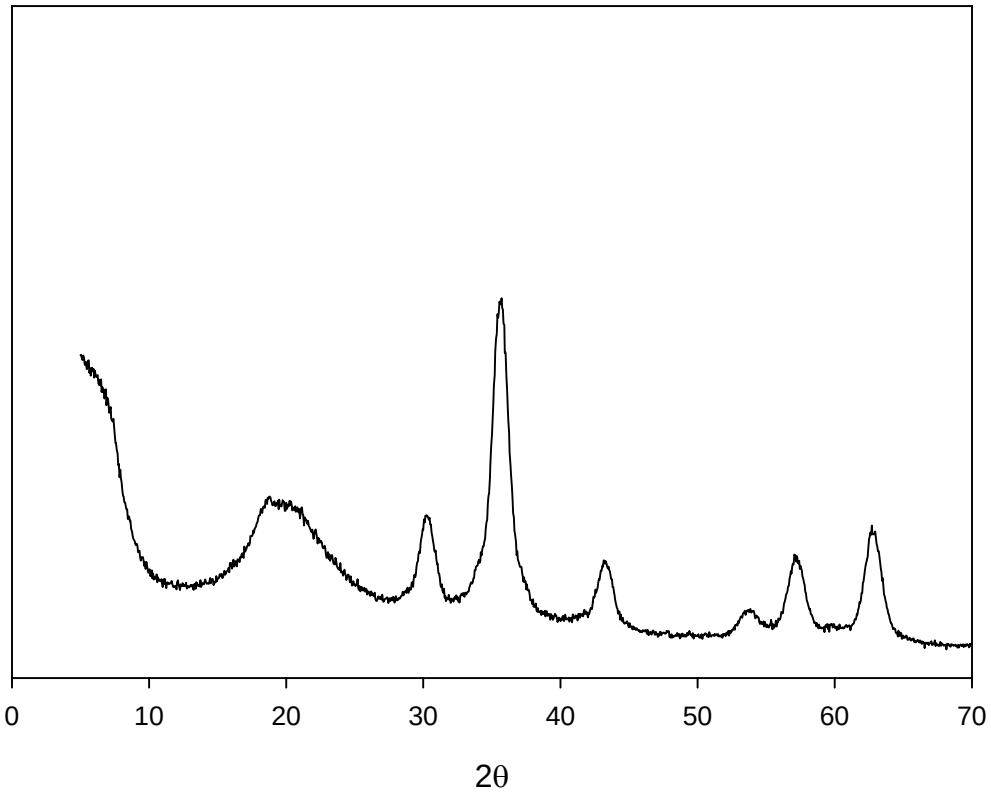


**Figure 3.19** XRD pattern from microwave polyol magnetite core-shell nanoparticle synthesis product prepared with 1,2-hexanediol and oleylamine co-capping agent

AFM and TEM analysis were performed on the sample (**Figure 3.20** and **Figure 3.21)**. Both indicate that spherical particles were formed. Based on these images, the particle sizes ranged from 9 –to 20 nm in diameter, which is in agreement with particle size estimates based on the XRD pattern. Repeat syntheses were performed with similar results.

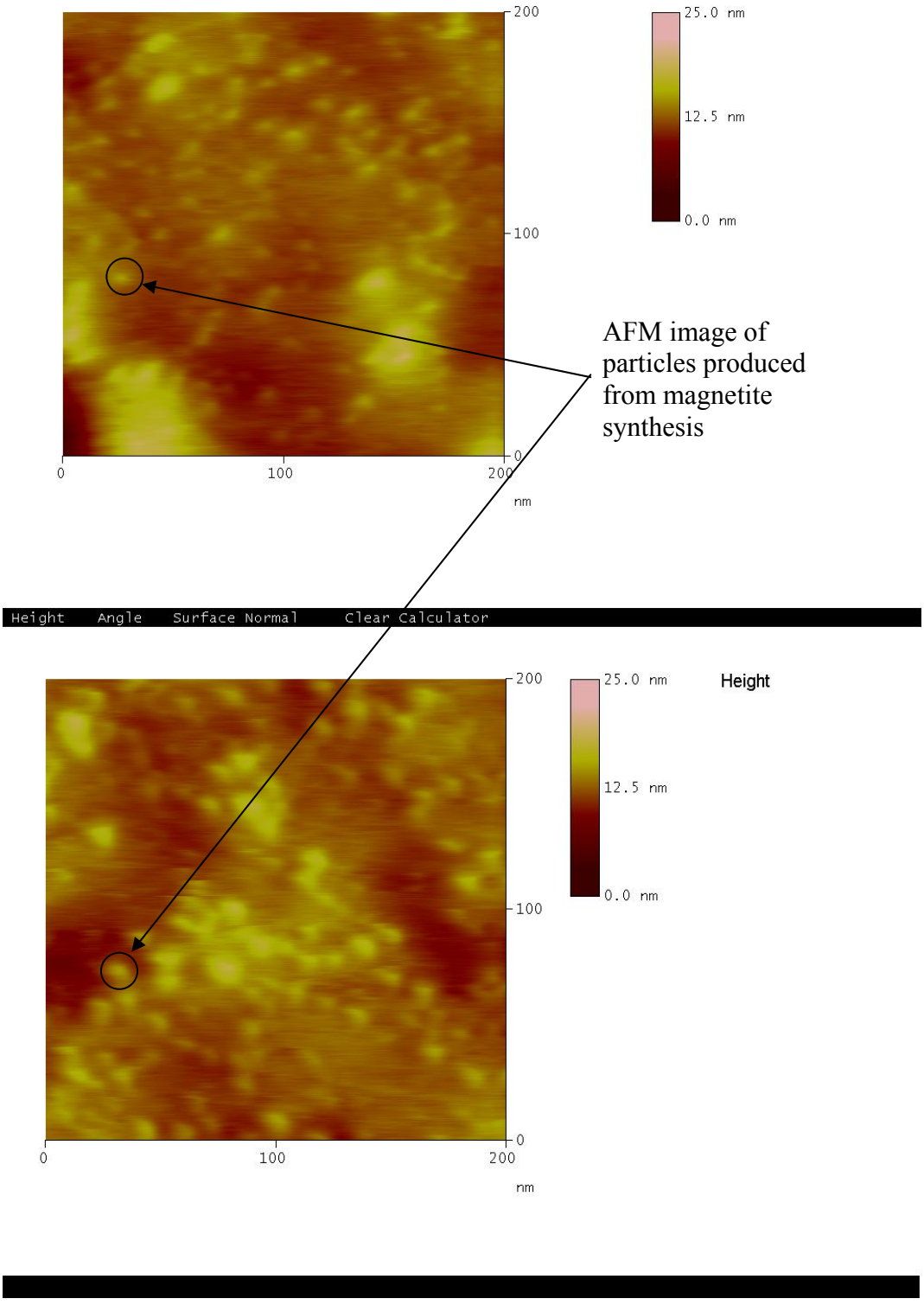


**Figure 3.20** Two AFM images of particles prepared via microwave polyol magnetite core-shell nanoparticle synthesis with 1,2-hexanediol and oleylamine co-capping agent

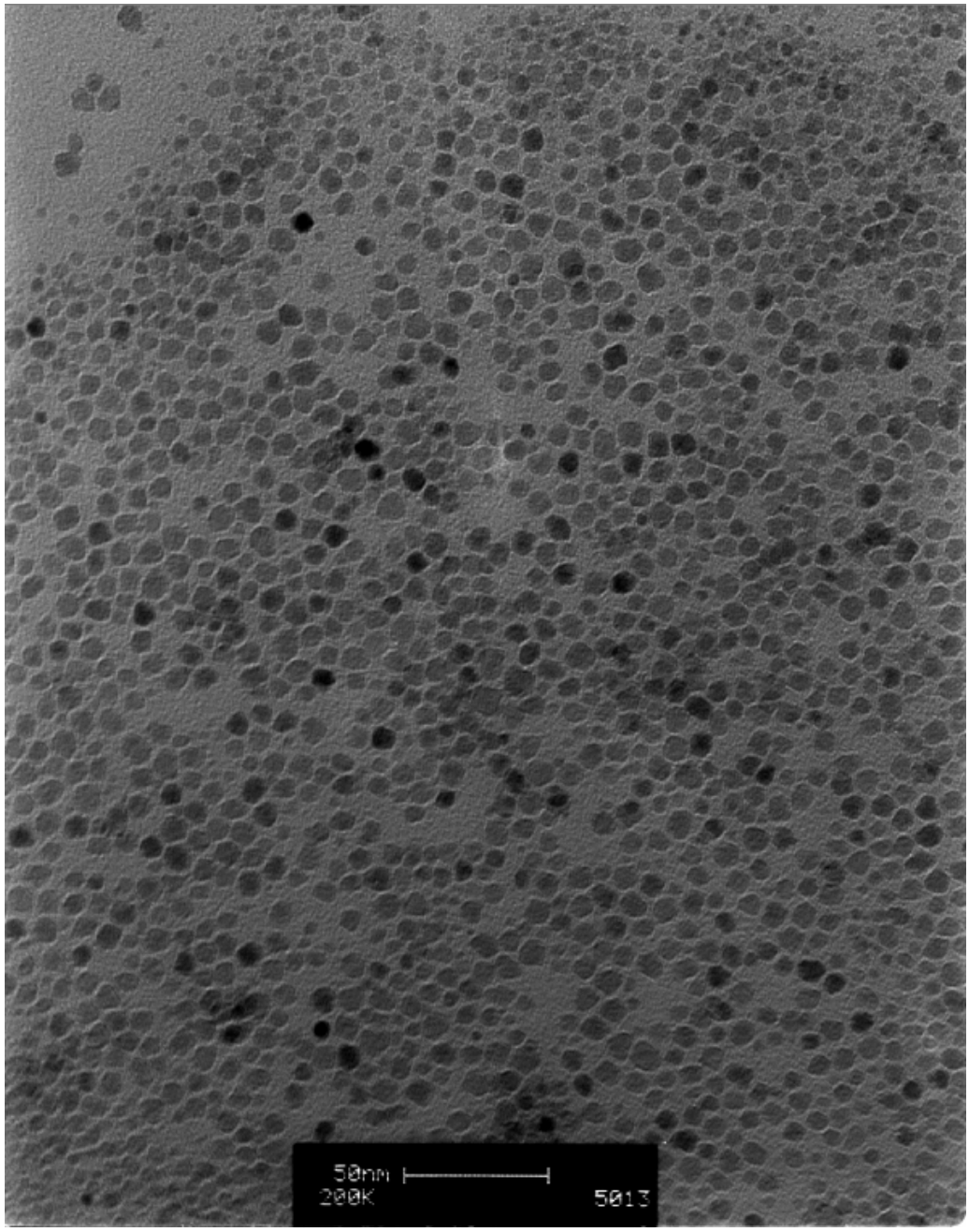


**Figure 3.21** TEM image of particles prepared via microwave polyol magnetite core-shell nanoparticle synthesis with 1,2-hexanediol and oleylamine co-capping agent

### 3.4 Microwave Time Investigation

To investigate the effect of time spent in the microwave, three identical reactions were performed varying only the reaction time. The reagents and reaction conditions are summarized in **Table 3.9**.

| Sample # | Type | Capping Agent | Reducing Agent | Solvent | Metal Salt | Variation |
|---|---|---|---|---|---|---|
| **MW1** | Fe | oleic acid | 1,2-hexadecanediol | octyl ether | $Fe(Acac)_2$ | increased to 50min |
| **MW2** | Fe | oleic acid | 1,2-hexadecanediol | octyl ether | $Fe(Acac)_2$ | reduced time to 20min |
| **MW3** | Fe | oleic acid | 1,2-hexadecanediol | octyl ether | $Fe(Acac)_2$ | reduced time to 10min |

**Table 3.9** Summary of microwave polyol time investigation reagents and conditions

**Figure 3.22** depicts the FT-IR spectra comparison of the products from the three microwave heating times, and they seem to show that the longer reaction times resulted in materials that displayed weaker bands in their FT-IR spectra. The XRD patterns from these reaction products were all similar, and all showed a magnetite structure.

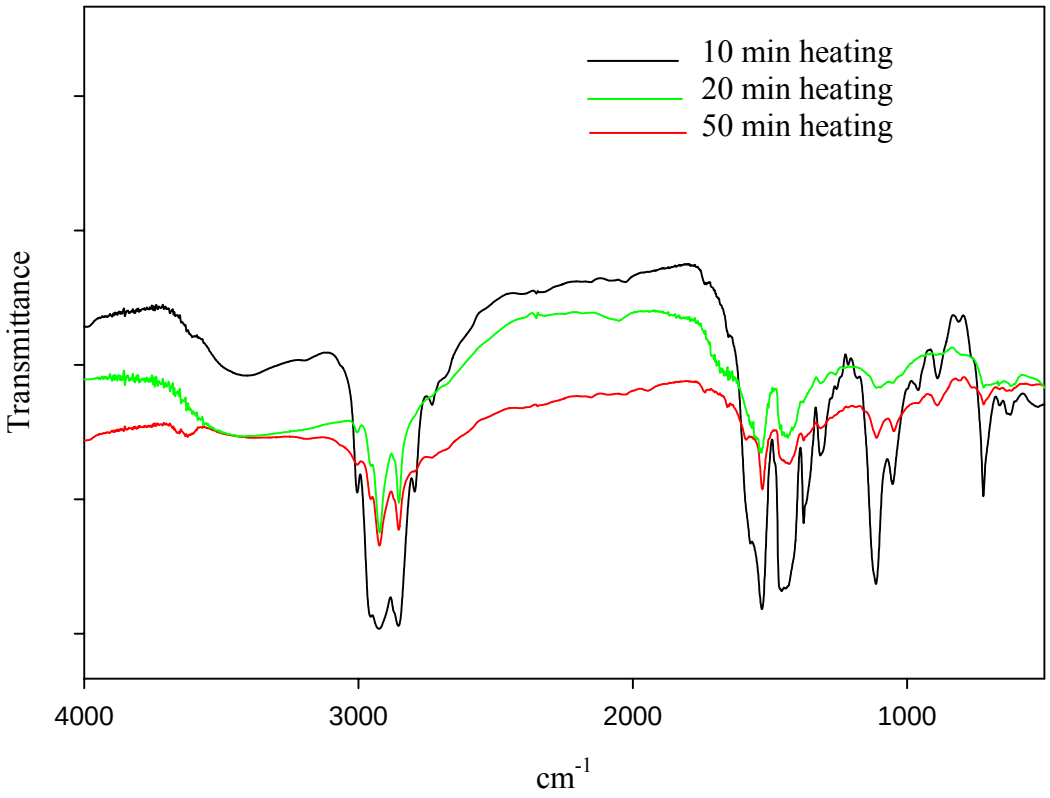


**Figure 3.22** FT-IR spectra comparison of three different microwave reaction times

### 3.4.1 TEM Size Comparison of Microwave Time Study

TEM was performed on the products from each reaction time. The particles produced from the 10 min reaction time (**Figure 3.23**) were noticeably smaller than those produced from the 50 min microwave reaction (**Figure 3.24**). From the TEM images, the particles from the 10 min microwave reaction are 5-7 nm, whereas the particles from the 50 min microwave reaction were 10-15 nm. This seems to indicate that the time spent in the microwave can affect the size of the particles produced. This also supports information from the literature that the number of particles produced is fixed.[14] The longer the particles were heated in the microwave, they only became larger, not greater in numbers.


**Figure 3.23** TEM image of 10 min microwave reaction

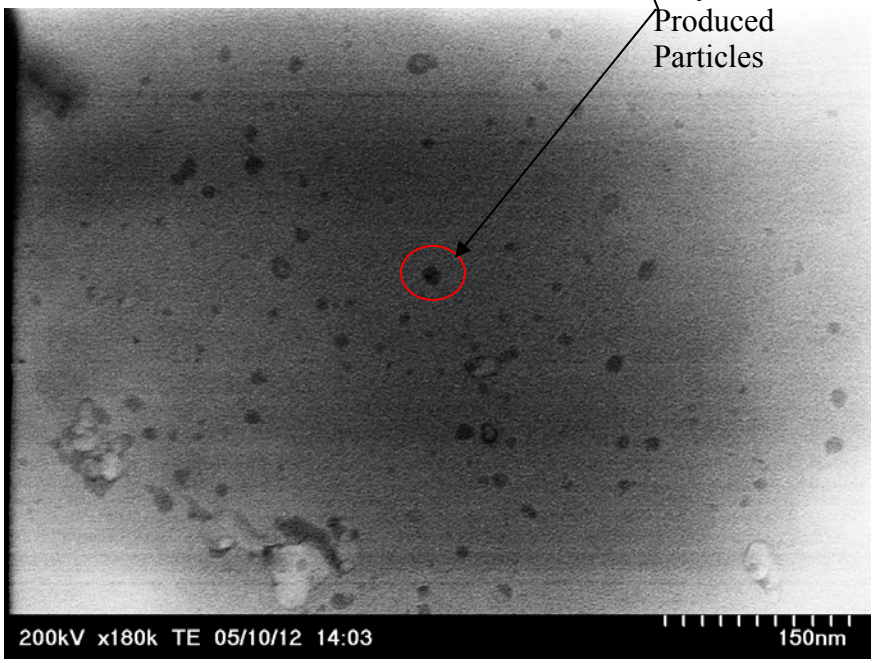


**Figure 3.24** TEM image of 50 min microwave reaction

### 3.5 Microwave Polyol $Co^0$ Core-shell Nanoparticle Synthesis Attempt

Having failed to conclusively produce $Fe^0$ core-shell nanoparticles via thermal and microwave polyol syntheses, our attention turned to microwave synthesis of $Co^0$ core-shell nanoparticles. $Co^0$ nanoparticle synthesis was attempted in order to verify that our microwave polyol method could indeed produce a fully reduced metal core nanoparticle. Based on reduction potentials, $Co^{+2}$ should be more easily reduced to $Co^0$ than $Fe^{+2}$ to $Fe^0$. **Table 3.10** summarizes the reaction conditions and reagents for these syntheses.

| Sample # | Type | Capping Agent | Reducing Agent | Solvent | Metal Salt | Variation |
|---|---|---|---|---|---|---|
| **MW1** | Co | oleic acid | 1,2-hexadecanediol | octyl ether | Co $(Acac)_2$ | |
| **MW2** | Co | oleic acid | 1,2-hexanediol | 1,2-hexanediol | Co $(Acac)_2$ | |
| **MW3** | Co | oleic acid | 1,2-hexanediol | 1,2-hexanediol | Co $(Acac)_2$ | stir bar left out |
| **MW4** | Co | oleic acid | 1,2-hexanediol | 1,2-hexanediol | Co $(Acac)_2$ | Repeat of MW2 |
| **MW5** | Co | oleic acid | 1,2-hexanediol | 1,2-hexanediol | Co $(Acac)_2$ | tripled capping agent concentration |

**Table 3.10** Summary of microwave polyol $Co^0$ nanoparticle syntheses reagents and conditions

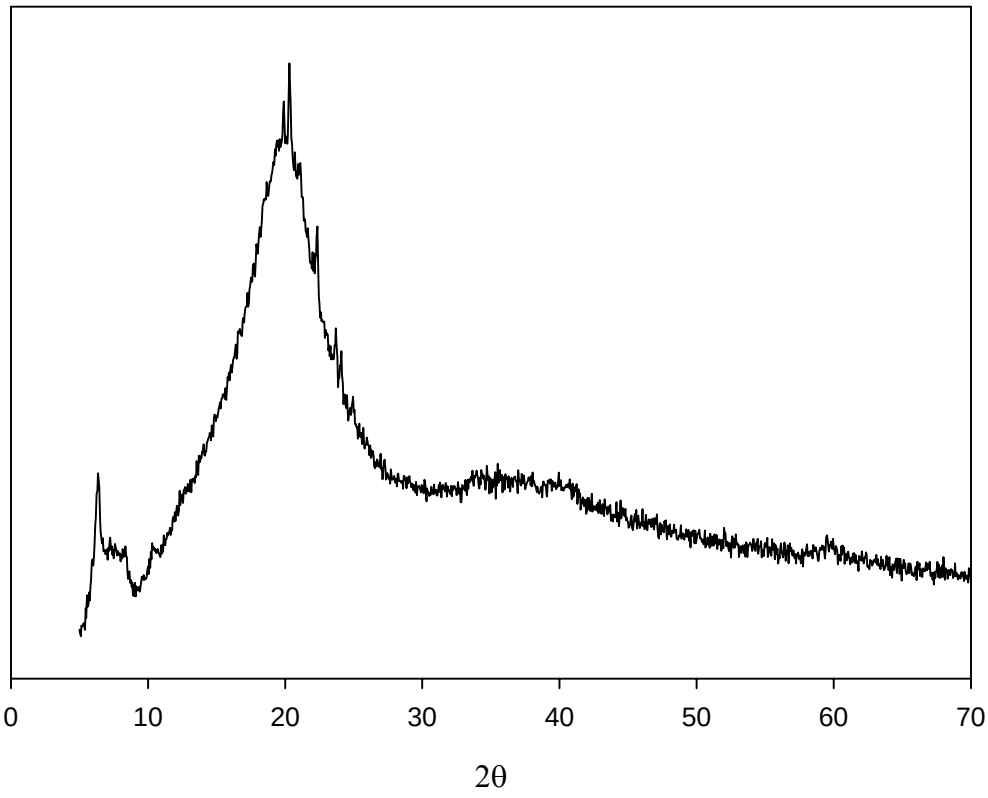


**Figure 3.25** XRD pattern of product from microwave polyol $Co^0$ core-shell nanoparticle synthesis

The product of this reaction was a purple wax, that when exposed to ambient conditions turned to a blue/black material The XRD pattern (**Figure 3.25**) looks similar to the previous microwave samples prepared in 1,2-hexanediol and PEG (**Figure 3.13** and **Figure 3.16**). Repeat syntheses were conducted, and similar results were obtained. Based on the XRD, it could not be determined that $Co^0$ core-shell nanoparticles were successfully produced. In order to conclusively identify the product as $Co^0$ two peaks at approximately 44° and 47° should be evident.[48] These two peaks are from a pure Co phase with hcp and fcc structures.[58] These two characteristic peaks are not evident in the XRD pattern of this product, but their presence can not be ruled out due to the elevated

baseline. The TEM images (**Figure 3.26**) confirm the presence of nanoparticles with sizes from 20-35 nm.

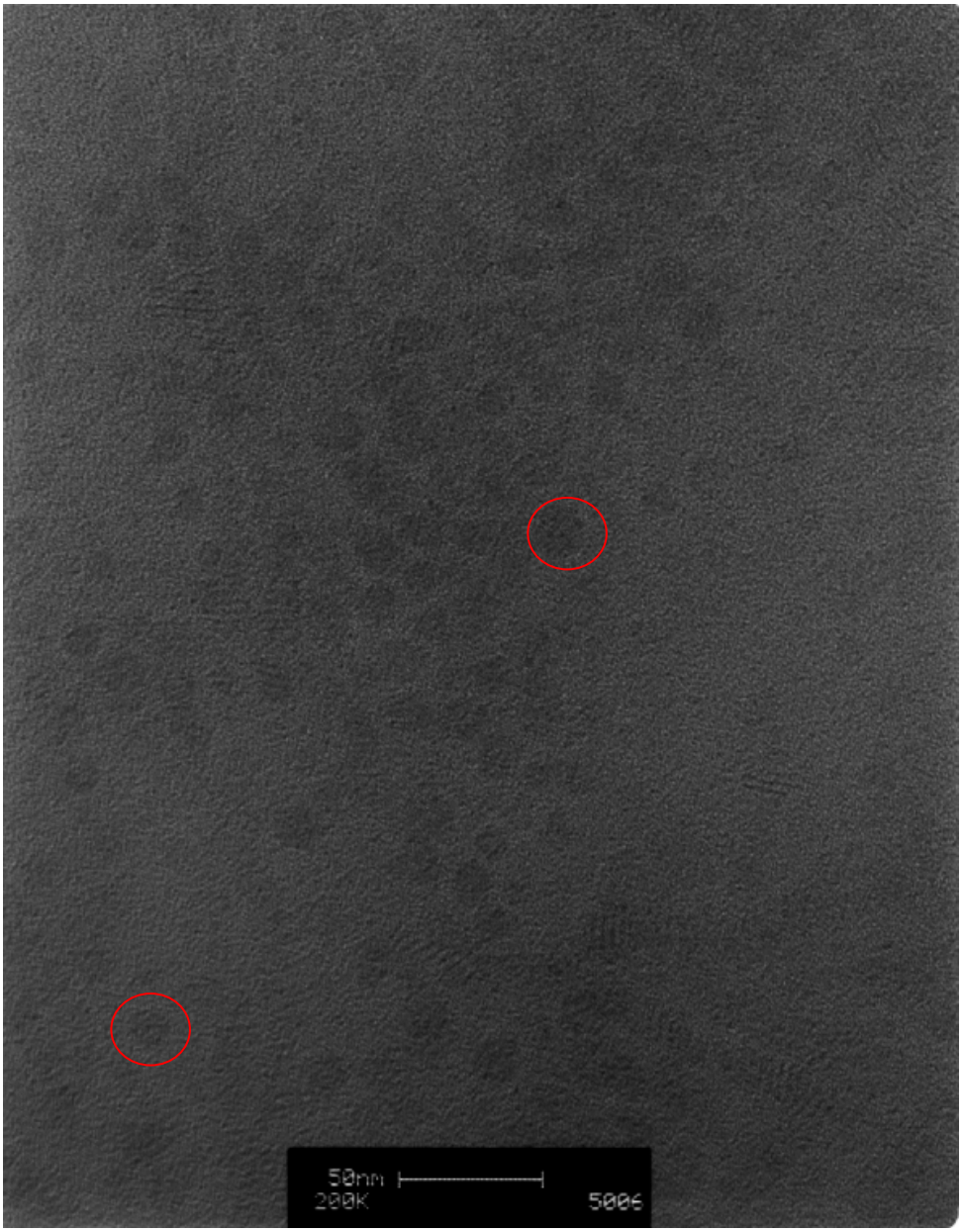


**Figure 3.26** TEM image of particles produced from microwave polyol $Co^0$ core-shell nanoparticle synthesis

### 3.6 Thermal and Microwave Investigation of Cobalt Co-reactant

Due to instrumentation limitations, no conclusive evidence was acquired for the formation of $Fe^0$ and $Co^0$ core-shell nanoparticles from both the thermal and microwave polyol reactions. There are many published reports of the polyol method producing $Fe^0$ particles, but these reactions were done in ethylene glycol.[14,35] Ethylene glycol was not investigated in this work, because it has been studied extensively, and there are many published articles on its use in the polyol method.

Thermal and microwave polyol reactions involving 1,2-hexadecanediol in octyl ether did produce magnetite core-shell nanoparticles. Because magnetite particles were produced fairly easily, a cobalt co-reactant was added to attempt to produce a FeCo oxide or, cobalt ferrite core-shell nanoparticle. The reaction conditions and reagents for these thermal reactions are summarized in **Table 3.11**.

| Sample # | Type | Capping Agent | Reducing Agent | Solvent | Metal Salt | Variation |
|---|---|---|---|---|---|---|
| **1** | Fe Co w/ $N_2$ | oleic acid | 1,2-hexadecanediol | octyl ether | Fe $(Acac)_2$ and Co $(Acac)_2$ | co-reactant |
| **2** | Fe Co w/ $O_2$ | oleic acid | 1,2-hexadecanediol | octyl ether | Fe $(Acac)_2$ and Co $(Acac)_2$ | co-reactant with air |
| **3** | Fe Co w/ $N_2$ | oleic acid | 1,2-hexadecanediol | octyl ether | Fe $(Acac)_2$ and Co $(Acac)_2$ | Repeat of #1 |
| **4** | Fe Co w/ $O_2$ | oleic acid | 1,2-hexadecanediol | octyl ether | Fe $(Acac)_2$ and Co $(Acac)_2$ | Repeat of #2 |

**Table 3.11** Summary of thermal polyol cobalt ferrite nanoparticle syntheses reagents and conditions

The first synthesis attempt was a thermal heating attempt in an ambient environment. This reaction resulted in a black powder rather than a wax. The black precipitate formed in this reaction responded to an external magnet and seemed to hold a

magnetic charge. The powder seemed to be magnetically attracted to itself and would ball up tightly when shaken. Based on previous FT-IR data from this research, it has been shown that the reaction successfully caps the resulting nanoparticles. Therefore, FT-IR analyses were not performed on the following set of reactions. The XRD pattern (**Figure 3.27**) indicates $CoFe_2O_4$ was formed based on comparison to the ICDD database. Repeat syntheses were performed with similar results. One Fe atom is replaced with one Co atom in the crystal lattice structure of $CoFe_2O_4$ as compared to $Fe_3O_4$. Even though a third of the metal atoms are different in the crystal lattice structure of cobalt ferrite, there is almost no difference in a magnetite XRD pattern and a cobalt ferrite XRD pattern.

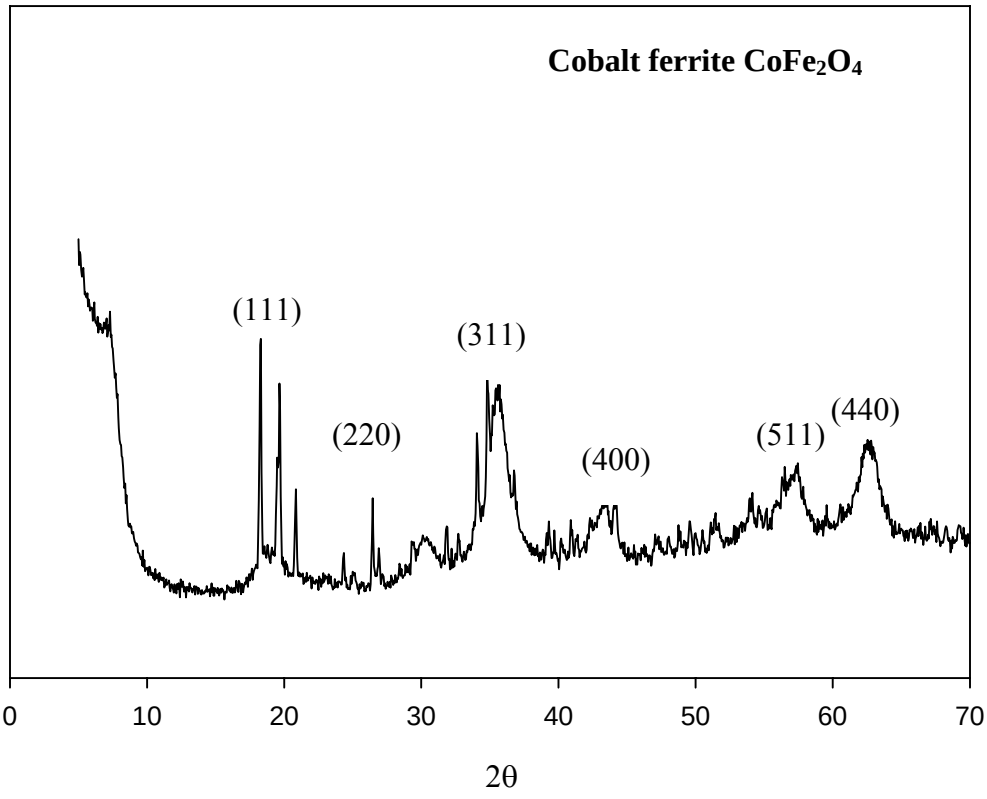


**Figure 3.27** XRD pattern of product from ambient thermal polyol $CoFe_2O_4$ core-shell nanoparticle synthesis with labeled Miller-index planes

In subsequent reactions, oxygen was eliminated from the reaction conditions. This product was a black wax. The XRD (**Figure 3.28**) revealed peaks that appear to be broader and less intense, and the baseline appears to show broad, underlying features.

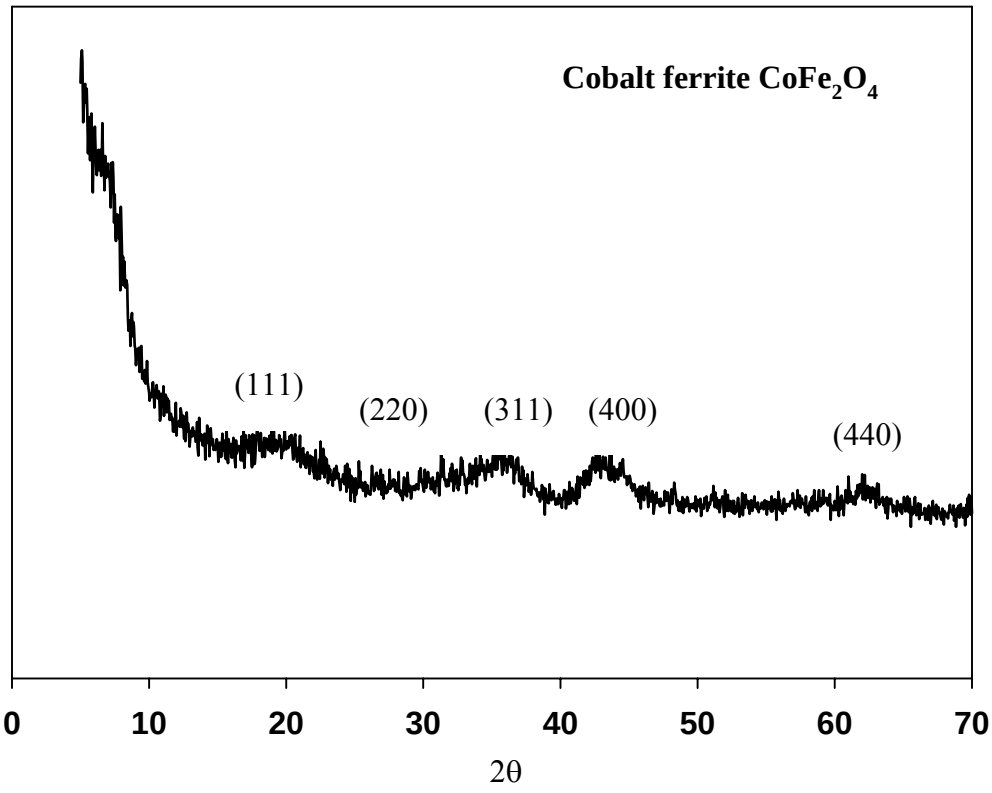


**Figure 3.28** XRD pattern of product from oxygen-free thermal polyol $CoFe_2O_4$ core-shell nanoparticle synthesis with labeled Miller-index planes

### 3.6.1 Microwave Polyol $CoFe_2O_4$ Core-shell Nanoparticle Synthesis

After the oxygen-free and ambient thermal reactions produced cobalt ferrite, microwave heating was investigated for this reaction, mirroring the $Fe^0$ core-shell particle syntheses. **Table 3.12** summarizes the reaction conditions and reagents for these syntheses.

| Sample # | Type | Capping Agent | Reducing Agent | Solvent | Metal Salt | Variation |
|---|---|---|---|---|---|---|
| **MW1** | FeCo | oleic acid | 1,2-hexadecane diol | octyl ether | Fe $(Acac)_2$ and Co $(Acac)_2$ | co-reactant |
| **MW2** | FeCo | oleic acid | 1,2-hexadecane diol | octyl ether | Fe $(Acac)_2$ and Co $(Acac)_2$ | Repeat of MW1 |

**Table 3.12** Summary of microwave polyol cobalt ferrite nanoparticle syntheses reagents and conditions

As with all microwave reactions, the reaction was performed under oxygen-free conditions. There was a low product yield and very little sample was available. The XRD pattern of the dark waxy product from this synthesis (**Figure 3.29**) is very noisy, and resembles that of the oxygen free thermal polyol cobalt ferrite synthesis (**Figure 3.28)**. TEM was run on this sample, and Energy Dispersive X-ray (EDX) was used to confirm the presence of both Co and Fe. From the TEM (**Figure 3.30**), the particle size seems similar the magnetite particles (**Figure 3.21**) and the $Co^0$ synthesis particles (**Figure 3.26**); around 20-25 nm. Repeat syntheses were performed and similar results were achieved.

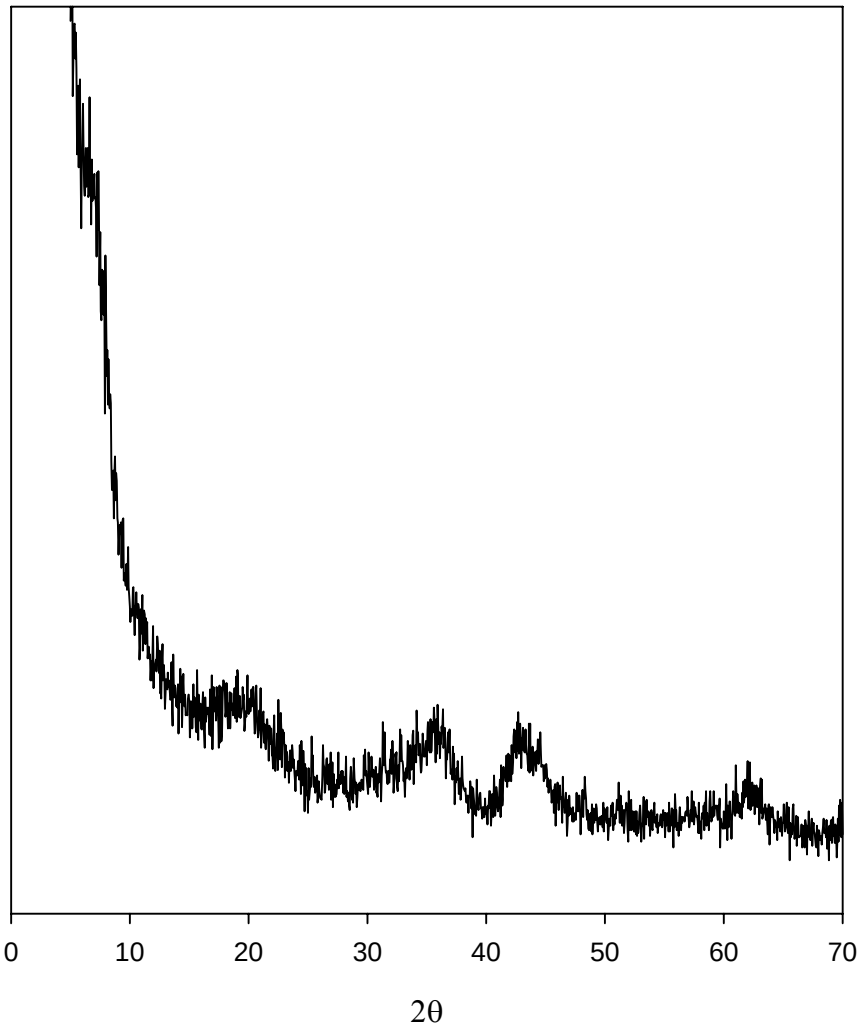


**Figure 3.29** XRD pattern of the product from microwave polyol $CoFe_2O_4$ core-shell nanoparticle synthesis


**Figure 3.30** TEM image of particles produced from microwave polyol $CoFe_2O_4$ core-shell nanoparticle synthesis

# IV CONCLUSIONS AND FUTURE WORK

In this study, both thermal and microwave polyol methods were investigated for the synthesis of iron, cobalt and iron-cobalt core-shell nanoparticles. Magnetite core-shell nanoparticles were synthesized via thermal heating based on published results. Attempts were made to synthesize $Fe^0$ core-shell nanoparticles via the same reaction by maintaining oxygen-free conditions. However, magnetite was again produced as confirmed by XRD analysis. It was also confirmed through FT-IR spectroscopic analysis that the oleic acid capping agent had formed a bond with the magnetite core. Microwave heating was then employed in an attempt to produce $Fe^0$ core-shell nanoparticles, because it was thought that localized hot spots created in the microwave could facilitate amorphous $Fe^0$ particle formation. However, magnetite was again produced, but the XRD pattern indicated the presence of smaller particles (around 2 nm) and possibly more amorphous particles.

Having produced only magnetite core-shell nanoparticles with both thermal and microwave polyol reactions using 1,2-hexadecanediol dissolved in octyl ether, two different polyol solvent/reducing agents were investigated. In order to reach higher reaction temperatures, 1,2-hexanediol and PEG MW 600 g/mol were chosen because they possess a large enough dielectric constant to efficiently absorb microwave energy. The syntheses performed with these two polyol solvents/reducing agents yielded products with significantly altered XRD patterns which displayed strong low-angle reflections that might be related to interlayer spacing in lamellar structures. Conspicuously absent was

the large peak at approximately 45°, which is an indicator of $Fe^0$. FT-IR was again used to confirm the presence of the capping agent on the metal core. TEM was used to confirm the formation of submicron-sized particles. Based on this information, it could not be determined that $Fe^0$ had been formed at any point in the reaction.

Microwave assisted reactions performed with 1,2-hexanediol did not produce a magnetite structure. Therefore, the synthesis of a magnetite core-shell nanoparticle using 1,2-hexanediol was carried out, but facilitated by the addition of an oleylamine co-capping agent. A magnetite core-shell nanoparticle was prepared successfully and its structure was verified using XRD.

Microwave assisted $Co^0$ core-shell nanoparticle synthesis was attempted and the XRD pattern from the product had the same strong low-angle reflection as the previous $Fe^0$ synthesis attempts with 1,2-hexanediol and PEG. The two large peaks at approximately 44° and 47°,which indicate $Co^0$, were not evident in the XRD pattern. Therefore, it could not be determined if $Co^0$ was produced.

The synthesis of $Fe^0$ core-shell nanoparticles was again attempted. The oxidation state of the iron precursor was changed for this synthesis from Fe (II) to Fe (III). Based on the reduction potentials of Fe (II) and Fe (III), Fe (III) is much easier to reduce than Fe (II) or even Co (II). The XRD patterns from the products of the syntheses exhibited identical features to those from the $Fe^0$ attempt with 1,2-hexanediol and PEG as well as the $Co^0$ synthesis. However, it could still not be concluded that $Fe^0$ had been produced.

Other parameters such as capping agent concentration, microwave time, and the addition of a cobalt co-reactant were investigated. The capping agent concentration appeared to have a limited effect on the particles produced, but the time spent in the

microwave seemed to have a significant effect on particle size. Longer reaction times afforded larger particles. A 10 min microwave reaction time produced particles in the 5-7 nm range, whereas the particles from the 50 min microwave reaction were 10-15 nm. When a cobalt co-reactant was introduced to the reaction, a cobalt ferrite structure was produced. All syntheses produced submicron particles with a protective surfactant layer.

Future avenues for this work could include the synthesis of human body-soluble, magnetic cobalt core-shell nanoparticles for use in drug delivery and resonance imaging. This could be facilitated by coating the particles with a protein. Because of the milder conditions provided by the microwave assisted polyol method, degradation of the protein capping agent might possibly be avoided. Also, the electrochemistry of the reduction mechanism of diols other than ethylene glycol could be investigated using linear sweep voltammetry.

## V REFFERENCES


(1) Bacha, J. et al. *Aviation Fuels Technical Review (FTR-3)*, Chevron Business and Real Estate Services Creative Center, San Ramon, CA, 2000

(2) Zabarnick, S.; Widmor, N. *Energy and Fuels* **2001**, *15*, 1447-1453

(3) Sun, S.; Murray, C.B. *J. Appl. Phy.* **1999**, *Vol. 85 No. 8*, 4325-4330 "Synthesis of monodisperse cobalt nanocrystals and their assembly into magnetic superlattices"

(4) Hyeon, T.; Lee, S.S.; Park, J.; Chung, Y.; Bin Na, H. *J. Am. Chem Soc.* **2001**, *123*, 12798-12801

(5) Pongkitwitoon, S. *Thermodynamics of Mixing for Nano-Particle Binary Mixing*; The Department of Materials Science and Engineering, Penn State, PA

(6) Wautelet, M.; Dauchot, J. P.; Hecq, M. *Nanotechnology* **2000**, *11*, 6-9

(7) Li, Z.; Chen, H.; Bao, H.; Gao, M. *Chem. Matter.* **2004**, *Vol. 16 No. 8*, 1391-1393 "One-Pot Reaction to Synthesize Water-Soluble Magnetite Nanocrystals"

(8) Kataby, G.; Cojocaru, M.; Prozorov, R.; Gedanken. A. *Langmuir* **1999**, *15*, 1703-1708 "Coating Carboxylic Acids on Amorphous Iron Nanoparticles"

(9) Allara, D.; Nuzzo, R. *Langmuir* **1985**, *1*, 45-52 "Spontaneously Organized Molecular Assemblies. 1. Formation, Dynamics, and Physical Properties of *n*-Alkanoic Acids Adsorbed from Solution on an Oxidized Aluminum Surface"

(10) Wu, N.; Fu, L.; Su, M.; Aslam, M.; Wong, K. C.; Dravid, V. P. *Nano Letters* **2004**, *Vol 4 No. 2*, 383-386 "Interaction of Fatty Acid Monolayers with Cobalt Nanoparticles"

(11) Harpeness, R. et al. *J. Colloid Interface Sci.* **2005**, *287*, 678-684 "Controlling the agglomeration of anisotropic Ru nanoparticles by the microwave-polyol process"

(12) Shafi, K. et al. *Langmuir* **2001**, *17*, 5093-5097 "Sonochemical Synthesis of Functionalized Amorphous Iron Oxide Nanoparticles"

(13) Grisaru, H.; Palchik, O.; Slifkin, M.A.; Weiss, A.M.; Gedanken, A. *Ingor. Chem.* **2003**, *42*, 7148-7155 "Microwave-Assisted Polyol Synthesis of $CuInTe_2$ and $CuInSe_2$ Nanoparticles"

(14) Fievet, F., Lagier, J.P.; Figlarz, M. *MRS Bull* **1989**, 29-34 "Preparing Monodisperse Metal Powders in Micrometer and Submicrometer Sizes by the Polyol Process"

(15) Bonet, F. et al. *Solid State Ionics* **1999**, *126*, 337-348 "Electrochemical reduction of noble metal species in ethylene glycol at platinum and glassy carbon rotating disk electrodes"

(16) Palchik, O.; Kerner, R.; Gedanken, A.; Weiss, A.M; Slifkin, M. A.; Palchik. V. *J. Mater. Chem.* **2001**,*11*, 874-878 "Microwave-assisted polyol method for the preparation of CdSe "nanoballs""

(17) Ying-Jie Zhu; Xian-Luo Hu *Materials Letters* **2004**, *58*, 1517-1519 "Microwave-assisted polythiol reduction method: a new solid-liquid route to fast preparation of silver nanowires"

(18) Kurihara, L.K.; Chow, G. M.; Schoen, P.E. *Nanostructured Materials* **1995**, *Vol. 5 No. 6*, 607-613 "Nanocrystaline Metallic Powders and Films Produced by the Polyol Method"

(19) Kerner, R.; Palchik, O.; Gedanken, A. *Chem. Mater.* **2001**, *13*, 1413-1419 "Sonochemical and Microwave-Assisted Preparations of PbTe and PbSe. A comparative study."

(20) Bonet, F.; Tekai-Elhsissen, K.; Vijaya Sarathy, K. *Bull. Mater. Sci.* **2000**, *Vol. 23 No. 3*, 165-168 "Study of interaction of ethylene glycol/PVP phase on noble metal powders prepared by polyol process"

(21) Sun, J. et al. *J. Matlet.* **2005**, "Mechanism of preparing ultrafine copper powder by polyol process"

(22) Viau, G.; Fievet-Vincent, F.; Fievet, F. *Solid State Ionics* **1996**, *84*, 259-270 "Nucleation and Growth of Bimetallic CoNi and FeNi Monodisperse Particles Prepared in Polyols"

(23) Galema S.A. *Chemical Society Reviews* **1997**, *26*, 233-238 "Microwave Chemistry"

(24) Echegoyen, L. et al. *Inorg. Chem.* **1993**, *32*, 572-577 "Formation of Cryptatium Species in Solution: Electrochemistry of Bipyridl-, Bipyrimidyl-, and Bithiazole-Based Cryptates"

(25) Gabriel, C.; Gabriel, S.; Grant, E.H.; Halstead, B.S.J; Mingos, D.M.P. *Chemical Society Reviews* **1998**, *27*, 213-223 "Dielectric Parameters Relevant to Microwave Dielectric Heating"

(26) Hayes, B. L. *Microwave Synthesis: Chemistry at the Speed of Light*; CEM Publishing, 2002

(27) Berlan, J. *Radiat. Phys. Chem*. **1995**, *Vol. 45 No.4*, 581-589 "Microwaves in chemistry: another way of heating reaction mixtures"

(28) Xian-Luo Hu; Ying-Jie Zhu; Shi-Wei Wang *Materials Chemistry and Physics* **2004**, *88*, 421-426 "Sonochemical and microwave-assisted synthesis of linked single-crystalline ZnO rods"

(29) Loupy, A. et al. *Pure Appl. Chem.* **2001**, *Vol. 73 No.1*, 161-166 "Reactivity and Selectivity Under Microwaves in Organic Chemistry. Relation with Medium Effects and Reaction Mechanisms"

(30) Mingos, D.M.P. *Res. Chem. Intermed.* **1994**, *Vol 20 No.1*, 85-91 "The Applications of Microwaves in Chemical Syntheses"

(31) Harpeness, R.; Gedanken, A. *Langmuir* **2004**, *20*, 3431-3434 "Microwave Synthesis of Core-Shell Gold/Palladium Bimetallic Nanoparticles"

(32) Komarneni, S.; Pidugu, R.; Li, Q. H.; Roy, R. *J. Mater. Res.* **1995**, *10*, 1687

(33) Caddick, S. *Tetrahedron* **1995**, *Vol.51 No. 38*, 10403-10432 "Microwave Assisted Organic Reactions"

(34) Komarneni, S.; Li, D.; Newalkar, B.; Katsuki, H.; Bhalla, A.S. *Langmuir* **2002**, *18*, 5959-5962 "Microwave-Polyol Process for Pt and Ag Nanoparticles"

(35) Komarneni, S.; Katsuki, H.; Li, D.; Bhalla, A. *J. Phys. Condens. Matter.* **2004**, *16*, S1305-S1312 "Microwave-polyol process for metal nanophases"

(36) Sun, S. et al. *J. Phys. Chem. B* **2003**, *107*, 5419-5425 "Controlled Synthesis and Assembly of FePt Nanoparticles"

(37) The mineral Magnetite Amethyst Galleries, Inc. (2006) http://mineral.galleries.com/minerals/OXIDES/MAGNETIT/magnetit.htm

(38) Sun, S.; Zeng, H. *J. Am. Chem. Soc.* **2002**, *124*, 8204-8205 "Size-Controlled Synthesis of Magnetite Nanoparticles"

(39) Cornell, R. M.; Schwertmann, U. *The Iron Oxides: Structure, Properties, Reactions, Occurrence and Uses* VCH: New York, 1996, pp28-29

(40) Hou, Y. et al. *J. Phys. Chem. B* **2005**, *109*, 4845-4852 "Inorganic Nanocrystal Self-Assembly via the Inclusion Interaction of β-Cyclodextrins: Toward 3D Spherical Magnetite"

(41) Kang, Y.S.; Risbud, S.; Rabolt, J.F.; Stroeve, P. *Chem. Mater.* **1996**, *8*, 2209-2211 "Synthesis and Characterization of Nanometer-Size $Fe_3O_4$and$\gamma$-$Fe_2O_3$ Particles"

(42) Cao, X.; Gu, L. *Nanotechnology* **2005**, *16*, 180-185 "Spindly cobalt ferrite nanocrystals: preparation, characterization and magnetic properties"

(43) Mallinson, J.C. *The Foundations of Magnetic Recording;* Academic: Berkeley, 1987; Chapter 3

(44) Neveu, S.; Bee, A.; Robineau, M.; Talbot, D. *J. Colloid and Interface Sciences* **2002**, *255*, 293-298 "Size-Selective Chemical Synthesis of Tartrate Stabilized Cobalt Ferrite Ionic Magnetic Fluid"

(45) Song, Q.; Zhang, Z. J. *J. Phys. Chem. B* **2006**, *110*, 11205-11209 "Correlation between Spin-Orbital Coupling and the Superparamagnetic Properties in Magnetite and Cobalt Ferrite Spinel Nanocrystals"

(46) Bunker, C.; Karnes, J. *J. Am. Chem. Soc.* **2004**, *126*, 10852-10853 "Low Temperature Stability and High Temperature Reactivity of Iron-Based Core-Shell Nanoparticles"

(47) Waser, Rainer (Ed.) *Nanoelectronics and Information Technology: Advanced Electronic Materials and Novel Devices.* Wiley-VCH GmbH & Co. KGaA, Germany. (2003) pg 276

(48) BRUKER AXS, D8 X-Ray Diffractometer User's manual Vol. 1 Karlsruhe, West Germany, 2002-2003

(49) Liu, C.; Wu, X.; Klemmer, T.; Shukla, N.; Yang, X.;Weller, D. *J. Phys. Chem. B* **2004**, *Vol. 108 No. 20*, 6121-6123 "Polyol Process Synthesis of Monodispersed FePt Nanoparticles"

(50) Whittaker, A.G.; Mingos, D.M.P. *J. Chem. Soc., Dalton Trans,* **2000**, 1521-1526 "Arcing and other microwave characteristics of metal powders in liquid systems"

(51) Larcher, D.; Sudant, G.; Patrice, R.; Tarascon, J.M. *Chem. Mater.* **2003**, *15*, 3543-3551 "Some Insights on the Use of Polyols-Based Metal Alkoxides Powders as Precursors for Tailored Metal-Oxides Particles"

(52) Shukla, N.; Liu, C.; Jones, P.M.; Weller, D. *Journal of Magnetism and Magnetic Materials*, **2003**, *266*, 178-184 "FTIR study of surfactant bonding to FePt nanoparticles"

(53) Yoon, S. et al. *Mater. Res. Soc. Symp. Proc.* **2005**, *848*, FF3.35.1-5 "The preparation of Ni nano particles by the chemically controlled polyol process"

(54) Klug, H.; Alexander, H.L. *X-ray Diffraction Procedures*; Wiley: New York, 1962; p 125

(55) Ennas, G. et al. *Chem. Mater.* **2004**, *16*, 5659-5663 "Influence of Metal Content on Size, Dispersion, and Magnetic Properties of Iron-Cobalt Alloy Nanoparticles Embedded in Silica Matrix"

(56) Stuerga, D.; Gaillard, P. *Tetrahedron* **1996**, *Vol. 52 No. 15,* 5505-5510 "Microwave heating as a new way to induce localized enhancements of reaction rate. Non-Isothermal and heterogeneous kinetics."

(57) Sun, S. et al. *J. Am. Chem. Soc.* **2004**, *126*, 273-279 "Monodisperse $MFe_2O_4$ (M=Fe, Co, Mn) Nanoparticles"

(58) Li, T.; Yang, S.; Huang, L.; Gu, B.; Du, Y.; *Nanotechnology* **2004**, *15*, 1479-1482 "A novel process from cobalt nanowire to $Co_3O_4$ nanotube"